PHYSICAL REVIEW C VOLUME 13, NUMBER 4 APRIL 1976

# Influence of virtual Δ states on the saturation properties of nuclear matter*

B. D. Day and F. Coester
*Argonne National Laboratory, Argonne, Illinois 60439*
(Received 22 December 1975)

The effect of virtual Δ(1236) states on the saturation properties of nuclear matter is studied within the framework of lowest-order Brueckner theory. The Δ is treated as a stable elementary particle. Transitions from the nucleon-nucleon ($NN$) channel to the nucleon-Δ ($N\Delta$) channel are caused by a nonrelativistic potential obtained from the static limit of meson theory. The coupled-channel potentials are constrained to fit the $NN$ phase shifts. Saturation curves are calculated for the couplings ${}^1S_0(NN) \rightleftarrows {}^5D_0(N\Delta)$ and ${}^3P_1(NN) \rightleftarrows {}^5P_1(N\Delta)$, and the effects of other $N\Delta$ couplings to nucleon-nucleon $P$ and $D$ waves are estimated. Calculations are done using both the Reid soft-core and Ueda-Green potentials for $NN$ partial waves not coupled to the $N\Delta$ channel. The $N\Delta$ coupling does not change the usual tendency of the calculated saturation points to lie in a narrow band in the energy-density plane that does not contain the empirical saturation point. This result is illuminated by a rough approximation to the Pauli and dispersion effects. We have also used this approximation to estimate the loss of binding due to $N\Delta$ coupling in those channels not treated by detailed calculation. Combining all our results, we find that at the empirical density (1) the inclusion of $N\Delta$ coupling in nucleon-nucleon $S$, $P$, and $D$ waves reduces the binding energy by about 3.3, 3.2, and 0.8 MeV, respectively, and (2) each particle spends about 3.7% of its time as a Δ. All these figures vary roughly quadratically with the $\pi N\Delta$ coupling constant and increase rapidly with density. The size of the shift in energy depends strongly on the suppression of the short-range part of the two-body wave function, but our approximate formulas indicate that the tendency of the calculated saturation points to remain in a narrow band is independent of the short-range behavior of the two-body interaction, i.e., it is model-independent.

[NUCLEAR STRUCTURE Effect of Δ(1236) on saturation of nuclear matter studied in lowest-order Brueckner-Bethe-Goldstone theory.]

## I. INTRODUCTION

For any nucleon-nucleon potential, the Brueckner-Bethe theory[1-3] predicts the saturation point, i.e., the equilibrium binding energy and density, of nuclear matter. For various potentials, the calculated saturation points lie on a narrow band in the energy-density plane, which we call the saturation band. The saturation band does not include the empirical saturation point, so that agreement with the empirical point can only be obtained by escaping from this band. The purpose of this paper is to learn whether the inclusion of intermediate nucleon-delta ($N\Delta$) states can permit an escape from the saturation band.

The main results of calculations with a variety of potentials are summarized in Fig. 1. In all calculations, the usual self-consistent single-particle spectrum[1] is used for states in the Fermi sea, and pure kinetic energy is used for states above the sea. Only two-body correlations are included in the calculation of the open and solid circles. Rough estimates[4] of the shift of the saturation point due to three- and four-hole-line corrections are shown by arrows for some of the potentials. The authors of the potentials and nuclear-matter calculations marked by solid circles are given in Table I. The open circles are new results, explained below. The tendency for the calculated saturation points to lie in a narrow band (the saturation band) is clear. The reason for this behavior has been discussed previously[5,6] for ordinary potentials without $N\Delta$ coupling.

The saturation band does not include the empirical saturation point, which lies within the box that extends in energy from −15 to −17 MeV and in Fermi momentum from 1.30 to 1.45 $\text{fm}^{-1}$. There are several possible reasons for this discrepancy. The convergence of the Brueckner-Bethe theory might be improved by a selective summation of higher-order terms, which would lead to a different single-particle spectrum from the one that is presently accepted.[8-10] Or, assuming the present Brueckner-Bethe theory to be correct, the evaluation of the three- and four-hole-line terms[11-13] might not be sufficiently accurate. Consequences of relativistic kinematics have also been considered, but a detailed study showed them to be negligible.[14] Finally, it may be inadequate to treat the nucleus as a system of point nucleons

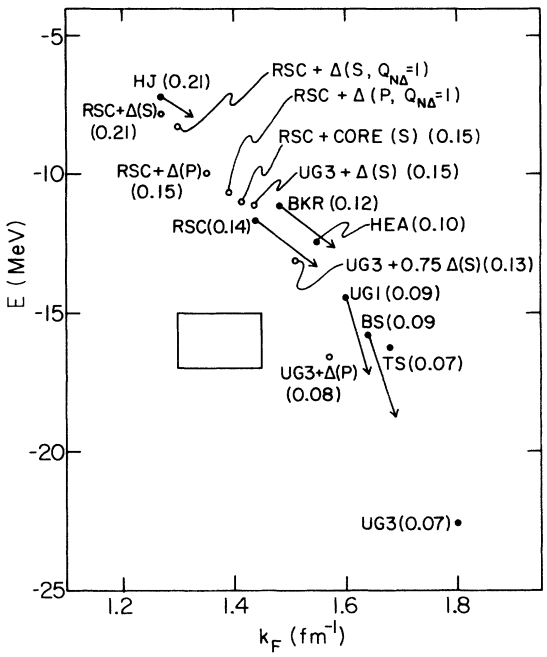


FIG. 1. Calculated saturation points for various models of the nucleon-nucleon interaction. The vertical axis is energy per particle in MeV, and the horizontal axis is Fermi momentum $k_F$ in fm$^{-1}$. The value of the dimensionless defect parameter $\kappa$ is given in parentheses. The quoted values of $\kappa$ are evaluated at $k_F = 1.36$ fm$^{-1}$, *not* at the saturation densities, in order to permit meaningful comparison between different potentials.

with no other explicit degrees of freedom. Meson and antinucleon degrees of freedom are, of course, buried in the phenomenological two-body potentials, but they may also have a distinct influence on the many-nucleon problem. In the absence of a complete fundamental theory, singling out particular degrees of freedom for explicit treatment need not be an improvement. The value of such models is primarily exploratory. They serve to point out the qualitative influence of a particular degree of freedom.

In this paper we treat the excited nucleon Δ(1236) as a stable elementary particle and assume a phenomenological interaction between Δ's and nucleons. The possible importance of this degree of freedom has been pointed out previously, especially by Green and co-workers.[15-17]

From earlier work on this isobar model[15-19] the following ideas have emerged. Ordinary nucleon-nucleon (*NN*) potentials are fitted to *NN* phase shifts. Hence they *implicitly* include the effect of coupling to the nucleon-delta (*N*Δ) channel. For example, this coupling produces a large attractive component in the usual $^1S_0$ *NN* potential. This attractive component is, of course, exactly the same, whether the potential is used for scattering or in nuclear matter. But when the *N*Δ channel is included *explicitly*, as in the isobar model, the coupling to this channel is less effective in nuclear matter than in the scattering problem. There are two reasons for this. First, when the two-body reaction matrix is computed in nuclear matter, the Pauli principle for the nucleons excludes certain *N*Δ intermediate states (Pauli effect). Second, the energy denominators for intermediate *N*Δ states are larger in nuclear matter than in the scattering problem (dispersion effect).

Rough calculations of the Pauli and dispersion effects, as functions of the density, have been made by Green and Niskanen.[17] They considered *N*Δ coupling in the $^1S_0$ channel of the Reid soft-core potential.[20] For a Fermi momentum $k_F = 1.4$ fm$^{-1}$, they found 5 MeV per particle less binding when *N*Δ coupling was included explicitly. They fitted their calculated loss of binding with the formula $0.702 k_F^{5.87}$.

In the present paper, we give the results of self-consistent Brueckner calculations with *N*Δ coupling explicitly included. Only two-body correlations are considered. For the $^1S_0$ channel of the Reid potential, our results are qualitatively similar to those of Green and Niskanen, but we find a somewhat smaller effect and a weaker density dependence. We find a much smaller Pauli effect than Green and Niskanen because they used a larger $\pi N\Delta$ coupling constant and neglected the dependence of the Pauli effect on the relative momentum of the two interacting nucleons. We will discuss their results in more detail in Sec. VI. Since we have done numerically accurate self-consistent calculations at various densities, we are in a better position to see whether inclusion of *N*Δ coupling moves the saturation point off the saturation band. The *P* waves in the *NN* channel may also be coupled to the *N*Δ channel, and there is no reason to assume that the effect of this coupling is negligible. In order to see whether *P*-wave coupling produces qualitatively different results, we have studied the effect of *N*Δ coupling in the $^3P_1$ channel with both the Reid potential and the Ueda-Green one-boson-exchange potential.[21] It turns out that the effect is comparable to the effect in the $^1S_0$ (*NN*) channel.

In Sec. II we specify the details of the model. In Sec. III, we discuss the scattering problem and introduce the two-body potentials. The calculation of the reaction matrix with *N*Δ coupling is described in Sec. IV, and the results of nuclear-matter calculations are presented in Sec. V. In Sec. VIA, we derive approximate formulas and verify their reliability by comparison with our detailed numerical results. We use these formulas in Sec. VIB to understand the main feature of the results, especially their variation with density

TABLE I. Authors of some of the nucleon-nucleon potentials and lowest-order nuclear-matter calculations shown in Fig. 1. Column one shows the symbol used for the potential in Fig. 1. Columns two and three give the authors of the potential and of the nuclear-matter calculation, respectively.

| Symbol | Authors of potential | Nuclear-matter calculation by |
|---|---|---|
| HJ | Hamada and Johnston [a] | Banerjee and Sprung [b] |
| BKR | Bressel, Kerman, and Rouben [c] | Banerjee and Sprung [b] |
| RSC | Reid soft-core [d] | Coester, Pieper, and Serduke [e] |
| HEA | Holinde, Erkelenz, and Alzetta [f] | Holinde, Erkelenz, and Alzetta [f] |
| UG1 | Ueda and Green [g] Model 1 | Wong and Sawada [h] |
| UG3 | Ueda and Green [g] Model 3 | Coester, Pieper, and Serduke [e] |
| BS | Bryan and Scott [i] | Wong and Sawada [h] |
| TS | DeTourreil and Sprung [j] | DeTourreil and Sprung [j] |

[a] Reference 28.
[b] Reference 7.
[c] C. Bressel, A. Kerman, and B. Rouben, Nucl. Phys. 124, 624 (1969).
[d] Reference 20.
[e] Reference 14.
[f] K. Holinde, K. Erkelenz, and R. Alzetta, Nucl. Phys. A198, 598 (1972).
[g] Reference 21.
[h] Reference 4.
[i] R. Bryan and B. L. Scott, Phys. Rev. 177, 1435 (1969).
[j] R. DeTourreil and D. W. L. Sprung, Nucl. Phys. A201, 193 (1973).

and their model dependence. In Sec. VI C we use the approximate formulas to estimate the effect of $N\Delta$ coupling in those channels not selected for detailed calculations. Our results are summarized in Sec. VII.

## II. DESCRIPTION OF THE MODEL

The specific model treated here is the one used earlier by Green and co-workers.[15-17] The Hamiltonian is

$$H=\sum_k \frac{\hbar^2k^2}{2M}\,a_k^\dagger a_k+\sum_k\left[\frac{\hbar^2k^2}{2\Delta}+(\Delta-M)c^2\right]\alpha_k^\dagger\alpha_k+\frac{1}{2}\sum_{klmn}\langle kl\,|V_1|\,mn\rangle a_k^\dagger a_l^\dagger a_n a_m+\sum_{klmn}\langle kl\,|V_3|\,mn\rangle a_k^\dagger\alpha_l^\dagger\alpha_n a_m$$
$$+\sum_{klmn}\left[\langle kl\,|V_2|\,mn\rangle a_k^\dagger\alpha_l^\dagger a_n a_m+\text{Hermitian conjugate}\right]. \qquad (1)$$

Here, $M$ is the nucleon mass and $\Delta$ is the mass of the $\Delta$. The operators $a_k$ and $a_k^\dagger$ destroy and create nucleons of momentum $k$, and the $\alpha_k$ and $\alpha_k^\dagger$ are analogous operators for the $\Delta$. The first two terms of formula (1) are the kinetic energies of nucleons and $\Delta$'s, along with the excitation energy $(\Delta-M)c^2$ of each $\Delta$ relative to the nucleon.

The two-body potentials $V_1$, $V_3$, and $V_2$ cause transitions of the types $NN \rightleftarrows NN$, $N\Delta \rightleftarrows N\Delta$, and $NN \rightleftarrows N\Delta$, respectively. The couplings $N\Delta \rightleftarrows \Delta\Delta$ and $NN \rightleftarrows \Delta\Delta$ are neglected because the mass of the $\Delta\Delta$ channel is 300 MeV greater than that of the $N\Delta$ channel. This does not imply that coupling to the $\Delta\Delta$ channel will have a negligible effect on the properties of nuclear matter. But by including only the $N\Delta$ channel, which is the single most important isobar channel, we expect to find out whether the inclusion of such channels can improve the saturation properties of nuclear matter. The $\Delta\Delta$ channel and all others are of course implicitly included in the model through the requirement that the $NN$ phase shifts be fitted.

The coupling potential $V_2$ must conserve two-body angular momentum $J$, parity $P$, and isospin $T$. This implies that the $^1S_0$ $NN$ channel is coupled only to the $^5D_0$ $N\Delta$ channel. Since the $^3S_1$ and $^1P_1$ $NN$ channels have $T=0$, they cannot couple to the $N\Delta$ channel, which has $T=1$ or 2. The $^3P$ ($NN$)

channels have $T=1$ and can couple to $N\Delta$ channels. In order to get an idea of the size and density dependence of the $N\Delta$ effect in $^3P$ channels, we have studied in detail the coupling of the $^3P_1$ ($NN$) channel to the $^5P_1$ ($N\Delta$) channel. We have also estimated the effect of other $P$-wave couplings. The effect of $N\Delta$ coupling on $NN$ channels with $L \geq 2$ is expected to be rather small and is discussed in Sec. VIC.

### III. SCATTERING PROBLEM AND POTENTIALS

We consider the interaction of two nucleons in a $NN$ channel that is explicitly coupled to a certain $N\Delta$ channel. The radial wave functions (multiplied by the relative distance $r$) in the $NN$ and $N\Delta$ channels are denoted by $u(r)$ and $w(r)$, respectively, and $L$ and $L'$ denote the respective orbital angular momenta. In the center-of-mass frame, the coupled Schrödinger equations for two-body scattering are

$$\left\{-\frac{\hbar^2}{M}\left[\frac{d^2}{dr^2}-\frac{L(L+1)}{r^2}\right]+V_1\right\}u+V_2 w=\frac{\hbar^2k^2}{M}u\,, \quad (2)$$

$$\left\{-\frac{\hbar^2}{2\mu}\left[\frac{d^2}{dr^2}-\frac{L'(L'+1)}{r^2}\right]+(\Delta-M)c^2+V_3\right\}w+V_2 u = \frac{\hbar^2k^2}{M}w\,. \quad (3)$$

Here, the reduced mass $\mu$ in the $N\Delta$ channel is given by

$$2\mu = 2M\Delta/(M+\Delta)\approx 1.14M\,, \quad (4)$$

and the energy eigenvalue in the center-of-mass system is

$$\hbar^2k^2/M=\tfrac{1}{2}E_{\rm lab}\,, \quad (5)$$

where $E_{\rm lab}$ is the scattering energy in the laboratory frame. Note that Eq. (3) for $w$ contains the $N\Delta$ mass difference $(\Delta-M)c^2$.

As $r\to 0$ (or as $r\to r_c$, in the case of an infinitely repulsive core of radius $r_c$), both $u$ and $w$ must vanish. For $E_{\rm lab}< 2(\Delta-M)c^2\cong 600$ MeV the $N\Delta$ channel is closed, and we have

$$u\sim \sin(kr+\tfrac{1}{2}L\pi+\delta) \quad \text{as } r\to\infty\,, \quad (6)$$

$$w\to 0 \quad \text{as } r\to\infty\,, \quad (7)$$

where $\delta$ is the $NN$ phase shift. The largest value of $E_{\rm lab}$ that we consider is 352 MeV, which is well below the $N\Delta$ threshold.

The potential $V_2(r)$ is obtained theoretically using the model of Sugawara and Von Hippel,[22] and $V_1$ and $V_3$ are then adjusted phenomenologically to fit the empirical $NN$ scattering phase shifts. We first review the calculation of $V_2$ and then give explicit formulas for the potentials.

The dominant contribution to $V_2$ comes from one-pion exchange (OPEP) and involves the OPEP amplitude $\langle N\Delta|\theta|NN\rangle$ for a transition from a $NN$ state to the state $|N\Delta\rangle$ in which particle 1 is a nucleon and particle 2 is a $\Delta$. The quantum numbers $LSJT$ of the states $|NN\rangle$ and $|N\Delta\rangle$ are suppressed for the moment but will be written when needed. In the static limit, $\theta$ is given by

$$\theta=\tfrac{1}{3}m_\pi c^2(ff^*/4\pi)\vec{\tau}_1\cdot\vec{\mathrm{T}}_2 \times[(1+3/x+3/x^2)S_{12}^{\rm II}+\vec{\sigma}_1\cdot\vec{\mathrm{S}}_2]e^{-x}/x\,, \quad (8)$$

where $m_\pi$ is the pion mass, $x=m_\pi r$, and $f$ and $f^*$ are the $\pi NN$ and $\pi N\Delta$ coupling constants, respectively. Also, $\frac{1}{2}\vec{\tau}_1$ is the isospin of nucleon 1, and $\vec{\mathrm{T}}_2$ changes the isospin of particle 2 from $\frac{1}{2}$ to $\frac{3}{2}$, corresponding to the $N\to\Delta$ transition for particle 2. Since $\vec{\mathrm{T}}_2$ is a spherical tensor of rank one, it can be defined by giving its reduced matrix elements in the isospin space of one particle, which can be either a nucleon (isospin $\frac{1}{2}$) or a $\Delta$ (isospin $\frac{3}{2}$). Its only nonzero reduced matrix element is (using the definition of reduced matrix element given by Edmonds[23]):

$$(\tfrac{3}{2}\|\,T_2\,\|\tfrac{1}{2})=2\,. \quad (9)$$

The analogous operators for the spin are $\frac{1}{2}\vec{\sigma}_1$ and $\vec{\mathrm{S}}_2$. The operator $S_{12}^{\rm II}$ is the analog of the usual tensor operator, i.e.,

$$S_{12}^{\rm II}=3\vec{\sigma}_1\cdot\hat{r}\vec{\mathrm{S}}_2\cdot\hat{r}-\vec{\sigma}_1\cdot\vec{\mathrm{S}}_2\,. \quad (10)$$

The matrix elements of $\vec{\tau}_1\cdot\vec{\mathrm{T}}_2$, $S_{12}^{\rm II}$, and $\vec{\sigma}_1\cdot\vec{\mathrm{S}}_2$ depend on the quantum numbers $LSJT$ and $L'S'JT$ of the initial $NN$ and final $N\Delta$ states, respectively. Explicit formulas for them are given by Sugawara and Von Hippel.[22] We have found, in agreement with Smith and Pandharipande,[24] that the Sugawara-Von Hippel formulas for matrix elements of $S_{12}^{\rm II}$ and $\vec{\sigma}_1\cdot\vec{\mathrm{S}}_2$ should be multiplied by $(-)^{S+S'+1}$ and $-1$, respectively.

Taking account of the fact that either nucleon 1 or nucleon 2 can be changed into a $\Delta$, one finds

$$V_2^{\rm OPEP}(r)=\tfrac{1}{3}\sqrt{2}\;m_\pi c^2(ff^*/4\pi) \times[\mathfrak{M}(1+3/x+3/x^2)e^{-x}/x+\mathfrak{N}e^{-x}/x]\,, \quad (11)$$

where $\mathfrak{M}$ and $\mathfrak{N}$ are defined by

$$\mathfrak{M}=\langle N\Delta, L'S'JT|(\vec{\tau}_1\cdot\vec{\mathrm{T}}_2)S_{12}^{\rm II}|NN, LSJT\rangle \quad (12)$$

and

$$\mathfrak{N}=\langle N\Delta, L'S'JT|(\vec{\tau}_1\cdot\mathrm{T}_2)\sigma_1\cdot\vec{\mathrm{S}}_2|NN, LSJT\rangle\,. \quad (13)$$

Some numerical values for $\mathfrak{M}$ and $\mathfrak{N}$ are given in Table II.

The values of $\mathfrak{M}$ in Table II motivate our selec-

tion of the couplings $^1S_0$ $(NN) \rightleftarrows {}^5D_0$ $(N\Delta)$ and $^3P_1$ $(NN) \rightleftarrows {}^5P_1$ $(N\Delta)$ for detailed study. Note first that the values of $\mathfrak{N}$ are relatively unimportant because the function multiplying $\mathfrak{N}$ in Eq. (11) is much smaller than the function that multiplies $\mathfrak{M}$. The $^1S_0(NN) \rightleftarrows {}^5D_0(N\Delta)$ coupling has a large value of $\mathfrak{M}$ and clearly must be studied. The contribution to the nuclear binding energy of the potential that couples a $^3P$ $(NN)$ channel to a particular $N\Delta$ channel should be roughly proportional to the square of $\mathfrak{M}$ and to the statistical weight $\frac{1}{8}(2T+1)(2J+1)$ of the $NN$ channel. Thus the contribution from coupling in the $^3P_0$ $(NN)$ channel is expected to be more than 10 times smaller than that from the $^3P_1$ $(NN) \rightleftarrows {}^5P_1$ $(N\Delta)$ coupling. The coupling $^3P_1$ $(NN) \rightleftarrows {}^5F_1$ $(N\Delta)$ has a large $\mathfrak{M}$, but coupling to $N\Delta$ channels with $L'=3$ should be less important than coupling to channels with $L'=1$. The same remark applies to the $^3P_2$ $(NN) \rightleftarrows {}^5F_2$ $(N\Delta)$ coupling, and the other $^3P_2$ $(NN)$ couplings have relatively small values of $\mathfrak{M}$. Thus we expect the coupling $^3P_1$ $(NN) \rightleftarrows {}^5P_1$ $(N\Delta)$ to be the single most important coupling involving a $^3P$ $(NN)$ channel.

Before the coupling potential of Eq. (11) is used in the Schrödinger equation, the $r^{-3}$ singularity must be removed. For the $^1S_0$ case, we have used the potential of Haapakoski,[25] who eliminates the $r^{-3}$ singularity by means of an infinitely repulsive core of radius $r_c = 0.4$ fm. If $r$ is measured in fm, the Haapakoski potentials outside the core are given in MeV by

TABLE II. Values of the matrix elements $\mathfrak{M}$ and $\mathfrak{N}$, defined by Eqs. (12) and (13) of the text, respectively. The total angular momentum, parity, and isospin of the channel are denoted by $J$, $P$, $T$, respectively. The usual spectroscopic notation is used to specify the values of $(LSJ)$ in the $NN$ channel and $L'S'J$ in the $N\Delta$ channel. Whenever an entry is omitted, the most recent entry above is to be understood.

| $NN$ channel | $J$ | $P$ | $T$ | $N\Delta$ channel | $\mathfrak{M}$ | $\mathfrak{N}$ |
|---|---|---|---|---|---|---|
| $^1S_0$ | 0 | + | 1 | $^5D_0$ | 4.000 | 0 |
| $^3P_0$ | 0 | − | 1 | $^3P_0$ | 1.333 | 2.667 |
| $^3P_1$ | 1 | − | 1 | $^3P_1$ | −0.667 | 2.667 |
| | | | | $^5P_1$ | 2.683 | 0 |
| | | | | $^5F_1$ | 2.191 | 0 |
| $^3P_2$ | 2 | − | 1 | $^3P_2$ | 0.133 | 2.667 |
| | | | | $^5P_2$ | −1.200 | 0 |
| | | | | $^3F_2$ | −0.980 | 0 |
| | | | | $^5F_2$ | 2.400 | 0 |
| $^1D_2$ | 2 | + | 1 | $^5S_2$ | 1.789 | 0 |

$$V_1(r) = V_3(r) = -10.5\,\frac{e^{-0.7r}}{0.7r} - 43\,\frac{e^{-2.75r}}{2.75r} + A\,\frac{e^{-3.9r}}{3.9r} - B\,\frac{e^{-2.1r}}{2.1r} \tag{14}$$

and

$$V_2(r) = 36.3y\left\{\frac{e^{-0.7r}}{0.7r}\left[1+\frac{3}{0.7r}+\frac{3}{(0.7r)^2}\right] - 220\,\frac{e^{-3.85r}}{3.85r}\left[1+\frac{3}{3.85r}+\frac{3}{(3.85r)^2}\right]\right\}. \tag{15}$$

Haapakoski chose the first three terms in formula (14) to represent the exchange of single $\pi$, $\eta$, and $\omega$ mesons, respectively. The last term in Eq. (14) represents two-pion-exchange effects that are not included through coupling to the $N\Delta$ channel. Putting $V_3$ equal to $V_1$ is arbitrary, but Green and Haapakoski[16] have shown that the phase shifts are very insensitive to the choice of $V_3$. The parameters $A$, $B$, and $y$ have been introduced for convenience in the following discussion.

Consider first the case $y=1$. The coupling potential $V_2$ is then precisely the one determined by Haapakoski.[25] The first term comes from $\pi$ exchange and is obtained from Eq. (11), using the values of $\mathfrak{M}$ and $\mathfrak{N}$ from Table II, along with $f^2/4\pi = 0.08$, $f^{*2}/4\pi = 0.23$. Haapakoski obtained this value of $f^*$ from a quark model; the observed width of the $\Delta$ leads to $f^{*2}/4\pi = 0.35$. The second term in Eq. (15) comes from $\rho$ exchange, and its derivation from a quark model is explained by Haapakoski.

Haapakoski adjusted $A$ and $B$ in Eq. (14) to fit the $^1S_0$ phase shifts. However, he used the approximation $2\mu = M$ in Eq. (3). Since we use the exact value given by Eq. (4), we have readjusted $A$ and $B$ to preserve a good fit to the phase shifts.

We have used values of $M$ and $\Delta$ obtained from the following constants:

$$\begin{aligned} &\hbar^2/M = 41.47 \text{ MeV fm}^2 , \\ &\hbar c = 197.32 \text{ MeV fm} , \\ &(\Delta - M)c^2 = 300 \text{ MeV} \quad (^1S_0 \text{ case}) , \\ &(\Delta - M)c^2 = 297.12 \text{ MeV} \quad (^3P_1 \text{ case}) . \end{aligned} \tag{16}$$

These values give about 1239 MeV for the mass of the $\Delta$ in the $^1S_0$ case. It would have been preferable to use the empirical mass of 1236 MeV, as was done in the $^3P_1$ case, but this small difference has a negligible effect on our results.

The $^1S_0$ scattering results are shown in Table III. Since we omit the Coulomb force, we have fitted our phase shifts to those predicted by the Reid soft-core potential[20] rather than to the $pp$ phase

TABLE III. Nucleon-nucleon phase parameters calculated without the Coulomb force for various $^1S_0$ potential models. In each of columns 1, 2, ··· 8 are given the parameters $y$, $A$, and $B$ of the potential (when appropriate), followed by the calculated scattering length $a$ and effective range $r_0$. Below these are given the phase shifts in radians for six different lab energies, e.g., $\delta(24)$ is the phase shift for $E_{lab} = 24$ MeV. Further details are given in the text.

| Column No. | 1 | 2 | 3 | 4 [a] | 5 | 6 | 7 | 8 |
|---|---|---|---|---|---|---|---|---|
| $y$ | | 1 | 1 | 1 | 0 | 0.25 | 0.50 | 0.75 |
| $A$ (MeV) | | 7175 | 7000 | 7000 | 1694 | 2069 | 3323 | 6008 |
| $B$ (MeV) | | 800 | 870 | 870 | 1290 | 1257 | 1175 | 1104 |
| $a$ (fm) | −17.1 | −17.3 | −246 | −25.9 | −17.2 | −17.2 | −17.1 | −17.2 |
| $r_0$ (fm) | 2.81 | 2.86 | 2.56 | 2.75 | 2.87 | 2.87 | 2.87 | 2.89 |
| $\delta$ (24) | 0.860 | 0.851 | 0.961 | 0.884 | 0.851 | 0.851 | 0.850 | 0.845 |
| $\delta$ (48) | 0.685 | 0.676 | 0.760 | 0.698 | 0.676 | 0.676 | 0.676 | 0.668 |
| $\delta$ (96) | 0.440 | 0.436 | 0.502 | 0.449 | 0.440 | 0.440 | 0.439 | 0.427 |
| $\delta$ (144) | 0.263 | 0.263 | 0.320 | 0.271 | 0.270 | 0.270 | 0.269 | 0.254 |
| $\delta$ (208) | 0.080 | 0.084 | 0.135 | 0.088 | 0.094 | 0.095 | 0.093 | 0.076 |
| $\delta$ (352) | −0.216 | −0.211 | −0.168 | −0.215 | −0.196 | −0.195 | −0.197 | −0.216 |

[a] Calculated by putting $2\mu = M$ in Eq. (3).

shifts. The Reid soft-core phase parameters are shown in column 1. In column 2 are shown our values of $A$ and $B$ for $y = 1$, along with the resulting phase parameters obtained by solving Eqs. (2) and (3). The quality of the fit is more than adequate for the present investigation.

Column 3 of Table III shows the values of $A$ and $B$ quoted by Haapakoski[25] for $y = 1$. The phase parameters in this column are obtained by using the exact reduced mass $\mu$ in Eq. (3) rather than the approximation $\mu = \frac{1}{2}M$ used by Haapakoski. The resulting phase parameters show that Haapakoski's original potential is somewhat too attractive when the exact reduced mass is used in the $N\Delta$ channel. If we set $\mu = \frac{1}{2}M$, then Haapakoski's values of $A$ and $B$ give a good fit to the phase parameters. These results are shown in column 4.

We have also fitted the phase shifts with weaker coupling potentials, corresponding to $y = 0.0$, 0.25, 0.50, and 0.75. For each value of $y$, $A$ and $B$ were adjusted to fit the phase shifts. These values of $A$, $B$ and the resulting phase parameters are shown in columns 5–8 of Table III. Such a sequence of potentials might be useful in studying the effect of varying the strength of the coupling potential. However, for our purposes it was sufficient to use $y = 0.0$, 0.75, and 1.0.

The coupling potential $V_2(r)$ is plotted for $y = 1$ in Fig. 2(a). Except at very short distances, it is seen to be comparable in strength to the rather strong Reid soft-core tensor force $\sqrt{8}\, V_T(r)$ that couples the $^3S_1$ and $^3D_1$ $NN$ channels. The potentials $V_1(r)$ corresponding to coupling strengths $y = 0$, 0.5, and 1.0 are plotted in Fig. 2(b). For $y = 1$, $V_1(r)$ is predominantly repulsive with a very weak attractive tail. Hence in this case nearly all the attraction comes from coupling to the $N\Delta$ channel. For $y = 0$, i.e., for no coupling, $V_1(r)$ is large and attractive outside the core. These facts show that the coupling for $y = 1$ is strong. The Reid hard-core $^1S_0$ potential[20] is also plotted in Fig. 2(b) for comparison with $V_1(r)$ for $y = 0$. The two potentials are seen to have nearly identical shapes. It is reasonable that the Reid potential is slightly more attractive because its core radius 0.423 fm is slightly larger than the core radius 0.4 fm used with $V_1(r)$.

For the coupling $^3P_1$ $(NN) \rightleftarrows {}^5P_1$ $(N\Delta)$, we have removed the $r^{-3}$ singularity from Eq. (11) by the phenomenological procedure of Reid,[20] which replaces the function multiplying $\mathfrak{M}$ in Eq. (11) by

$$Z(x) \equiv (1 + 3/x + 3/x^2)e^{-x}/x - (12/x + 3/x^2)e^{-4x}/x \,. \tag{17}$$

Formula (17) agrees with Eq. (11) at large $r$ and has only an $r^{-1}$ singularity at $r = 0$. Pieper[26] has found that $Z(x)$ is accurately approximated by the function

$$Y(x) \equiv 1.7728e^{-x}/x + 10.447e^{-2x}/x + 13.493e^{-4x}/x - 2.2124e^{-6x}/x \,, \tag{18}$$

and we have used this formula in our calculations. In applications where momentum-space matrix elements of $V_2$ are needed, they are more easily calculated using the function $Y$ than the function $Z$.

Measuring the potential in MeV and $r$ in fm, we obtain for the coupling ${}^3P_1$ $(NN) \rightleftarrows {}^5P_1$ $(N\Delta)$,

$$V_2(r) = 30yY(0.7r) \ . \tag{19}$$

The parameter $y$ is introduced to allow variation of the coupling strength. Using Eq. (11) with Haapakoski's[25] values of $f$ and $f^*$ and taking $\mathfrak{M}$ from Table II gives Eq. (19) with $y = 1$. We have also used

$$V_1(r) = V_3(r) = 10.463[\,(1 + 2/x + 2/x^2)e^{-x}/x - (8/x + 2/x^2)e^{-4x}/x] + a_2 e^{-2x}/x + a_4 e^{-4x}/x + a_6 e^{-6x}/x \ , \tag{20}$$

where $x = 0.7r$. The first term is OPEP with Reid's removal of the $r^{-3}$ singularity. The coefficients $a_2$, $a_4$, and $a_6$ are adjusted to fit the ${}^3P_1$ phase shifts obtained from the Reid soft-core ${}^3P_1$ potential with the Coulomb force neglected.

We have fitted the ${}^3P_1$ phases in this way for $y = 0.75$, 1.0, and 1.5. The results are shown in Table IV. The fits are seen to be very good. The coupling potential (19), with $y = 1$, is plotted in Fig. 2(a) and is seen to be comparable to the rather strong coupling between the ${}^1S_0$ $(NN)$ and ${}^5D_0$ $(N\Delta)$ channels.

## IV. CALCULATION OF THE REACTION MATRIX

For $NN$ channels without $N\Delta$ coupling, the reaction matrix is computed in momentum space using the angle-average Pauli operator. The method is described by Coester, Pieper, and Serduke.[14]

For the channels with $N\Delta$ coupling, the method of Kallio and Day[27] has been used, also with the angle-average Pauli operator. The coupled-channel equations have the same structure as those for the usual tensor-coupled channels, e.g., the ${}^3S_1$-${}^3D_1$ channel. Thus we simply use the tensor-coupled Kallio-Day equations, with modifications to take account of (1) the $\Delta$-$N$ mass difference and (2) the different Pauli operator that must be used in the $N\Delta$ channel. We now give a brief outline of the method and then present the resulting equations that have been used in our numerical work.

The correlated two-body wave function $\psi$ satisfies

$$\psi = \phi - (Q/e)V\psi \tag{21}$$

or

$$(-e - V)\psi = -e\phi - (1 - Q)V\psi \ , \tag{22}$$

where $\phi$ is the uncorrelated plane wave, and the Pauli operator $Q$ requires nucleon momenta to be outside the Fermi sea but allows the $\Delta$ to have any momentum. The operator $e$ is given by

$$e = E_1 + E_2 - W \ , \tag{23}$$

where $E_i$ is the energy of particle $i$, and $W$ is the two-body starting energy. For nucleons, $E_i$ is pure kinetic energy, and for $\Delta$'s it is kinetic energy plus the mass difference $(\Delta - M)c^2$.

In the Kallio-Day method, Eq. (22) is written in partial-wave representation in coordinate space and solved iteratively. In the first iteration the second term on the right is neglected, and the resulting differential equation is solved for $\psi$. This approximate $\psi$ is then used to evaluate $(1 - Q)V\psi$, which is treated as a known inhomogeneous term, and Eq. (22) is solved again to get a better approximation to $\psi$. This process usually converges in four and five iterations.

Because of the $\Delta$-$N$ mass difference, the operator $e$ takes different forms $e_{NN}$ and $e_{N\Delta}$ in the $NN$ and $N\Delta$ channels, respectively:

$$e_{NN} = -\frac{\hbar^2}{M}\nabla^2 + \frac{\hbar^2}{4M}P^2 - W = \frac{\hbar^2}{M}(\gamma_0^{\,2} - \nabla^2) \ , \tag{24}$$

$$e_{N\Delta} = -\frac{\hbar^2}{2\mu}\nabla^2 + \frac{\hbar^2}{2(M+\Delta)}P^2 + (\Delta - M)c^2 - W = \frac{\hbar^2}{2\mu}(\gamma_2^{\,2} - \nabla^2) \ , \tag{25}$$

where $P$ is the two-body center-of-mass momentum. Equations (24) and (25) serve to define $\gamma_0^{\,2}$ and $\gamma_2^{\,2}$, respectively.

The angle-average Pauli operator $Q$ also has different forms $Q_{NN}$ and $Q_{N\Delta}$ in the $NN$ and $N\Delta$ channels, respectively. This is because in the $N\Delta$ channel only the nucleon is required to be above the Fermi sea. In Eq. (22), we need $\mathcal{P} \equiv 1 - Q$, and for the $NN$ channel we have the standard result

$$\begin{aligned} \mathcal{P}_{NN}(k,P) &= 1, \quad k < (k_F^{\,2} - \tfrac{1}{4}P^2)^{1/2} \\ &= 0, \quad k > k_F + \tfrac{1}{2}P \\ &= 1 - (k^2 + \tfrac{1}{4}P^2 - k_F^{\,2})/kP, \quad \text{otherwise} \ , \end{aligned} \tag{26}$$

where $k$ is the relative momentum, and $k_F$ is the Fermi momentum. In the $N\Delta$ channel one easily finds

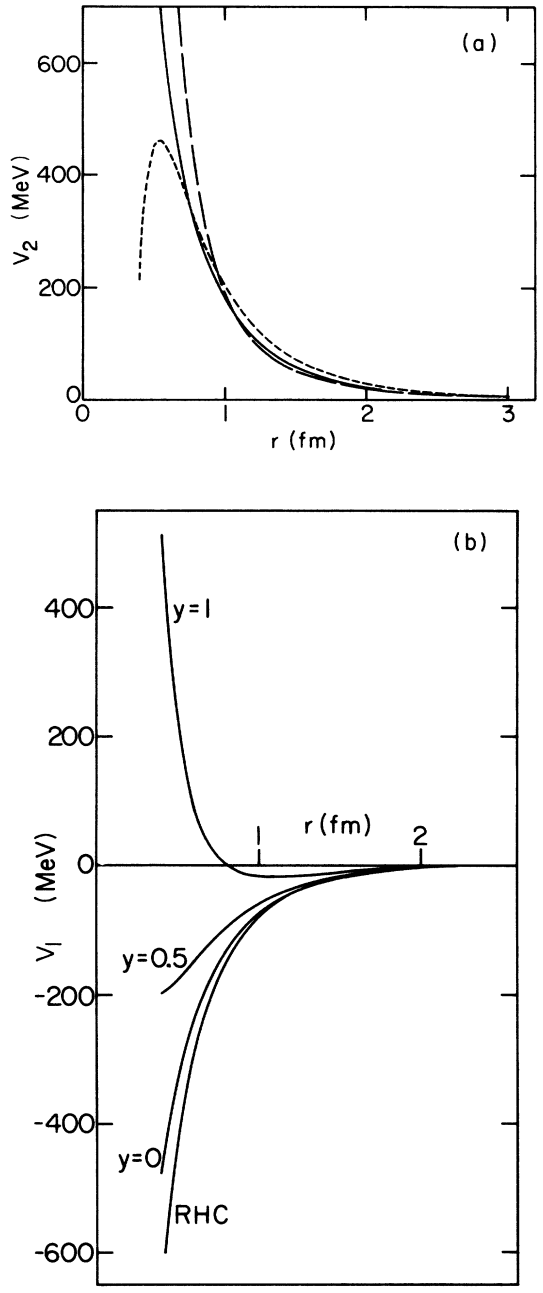


FIG. 2. (a) Coupling potentials $V_2$ vs relative distance $r$. The short-dashed curve is for the coupling ${}^1S_0(NN) \rightleftarrows {}^5D_0(N\Delta)$ and is obtained from Eq. (15) with $y=1$. The solid curve is for the coupling ${}^3P_1(NN) \rightleftarrows {}^5P_1(N\Delta)$ and is obtained from Eq. (19) with $y=1$. For comparison, the long-dashed curve gives $-8^{1/2}V_T(r)$, where $V_T(r)$ is the ${}^3S_1 - {}^3D_1$ tensor force of the Reid soft-core potential. (b) Potentials $V_1$ vs relative distance $r$ for various coupling strengths $y$ in the case ${}^1S_0(NN) \rightleftarrows {}^5D_0(N\Delta)$. The curve labeled RHC is the ordinary Reid hard-core ${}^1S_0$ potential.

TABLE IV. Nucleon-nucleon phase shifts in the ${}^3P_1$ channel calculated with the Coulomb force omitted. Column 1 gives the phases in radians at various lab energies for the Reid soft-core potential. Columns 2, 3, and 4 give the results for potentials with $N\Delta$ coupling, as defined by Eqs. (19) and (20) of the text.

| Column No. | 1 | 2 | 3 | 4 |
|---|---|---|---|---|
| $y$ | | 1.0 | 0.75 | 1.5 |
| $a_2$ (MeV) | | −95.07 | −93.77 | −94.89 |
| $a_4$ (MeV) | | 1641.9 | 1363.8 | 2338.4 |
| $a_6$ (MeV) | | 229.9 | −22.14 | 894.84 |
| $\delta$ (10) | −0.034 | −0.034 | −0.034 | −0.034 |
| $\delta$ (25) | −0.080 | −0.080 | −0.080 | −0.080 |
| $\delta$ (50) | −0.142 | −0.141 | −0.141 | −0.141 |
| $\delta$ (100) | −0.240 | −0.238 | −0.237 | −0.239 |
| $\delta$ (175) | −0.350 | −0.351 | −0.351 | −0.352 |
| $\delta$ (250) | −0.434 | −0.436 | −0.437 | −0.435 |
| $\delta$ (350) | −0.520 | −0.518 | −0.524 | −0.514 |

$$\begin{aligned} \mathcal{P}_{N\Delta}(k,P) &= 1, \quad k < k_F - MP/(M+\Delta) \\ &= 0, \quad k > k_F + MP/(M+\Delta) \\ &= [4kMP/(M+\Delta)]^{-1} \\ &\quad \times \left[ k_F^2 - \left( \frac{MP}{M+\Delta} - k \right)^2 \right] \text{ otherwise .} \end{aligned} \tag{27}$$

In Eqs. (26) and (27) it is assumed that $P \leq 2k_F$; only this case occurs in our calculations.

The Kallio-Day derivation can now be easily carried through, and we give the resulting equations below, using the following notation. The correlated radial wave functions (all radial functions are multiplied by $r$) in the $NN$ and $N\Delta$ channels are denoted by $u$ and $w$, respectively. These channels have respective orbital angular momenta $L$ and $L'$. The uncorrelated plane wave $\exp(i\vec{k}_0 \cdot \vec{r})$ has only a $NN$ component, given by $rj_L(k_0 r)$. The partial-wave components of $(1-Q)V\psi$ in the $NN$ and $N\Delta$ channels are called $F_{NN}(r)$ and $F_{N\Delta}(r)$, respectively. The equations used in computation are then (in units with $\hbar^2/M = 1$, so that 1 fm$^{-2}$ = 41.47 MeV):

$$\left[ \frac{d^2}{dr^2} - \frac{L(L+1)}{r^2} - \gamma_0^2 - V_1 \right] u - V_2 w = -(k_0^2 + \gamma_0^2) r j_L(k_0 r) - F_{NN}(r) \tag{28}$$

and

$$\left[ \frac{d^2}{dr^2} - \frac{L'(L'+1)}{r^2} - \gamma_2^2 - bV_3 \right] w - bV_2 u = -bF_{N\Delta}(r) , \tag{29}$$

where

$$b = 2\mu/M \ . \tag{30}$$

The boundary conditions are

$$u(r) = w(r) = 0, \quad r \le r_c , \tag{31}$$

$$u(r) \to rj_L(k_0 r), \quad \text{as } r \to \infty , \tag{32}$$

$$w(r) \to 0, \quad \text{as } r \to \infty , \tag{33}$$

where $r_c$ is the radius of the hard core in the two-body potential (the possibility $r_c = 0$ is not excluded).

Also

$$F_{NN}(r) = \frac{1}{2\pi^2} \int k^2 dk \, \varphi_{NN}(k, P) \times (k, NN|G|k_0, NN) r j_L(kr) , \tag{34}$$

$$F_{N\Delta}(r) = \frac{1}{2\pi^2} \int k^2 dk \, \varphi_{N\Delta}(k, P) \times (k, N\Delta|G|k_0, NN) r j_{L'}(kr) , \tag{35}$$

where the elements of the reaction matrix $G$ are given by

$$(k, NN|G|k_0, NN) = 4\pi(\gamma_0^2 + k_0^2) \int_0^{r_c} j_L(kr) j_L(k_0 r) r^2 dr + 4\pi \int_0^{r_c} r j_L(kr) F_{NN}(r) dr + 4\pi r_c j_L(kr_c) \left.\frac{du}{dr}\right|_{r_c} + 4\pi \int_{r_c}^{\infty} r j_L(kr)[V_1 u + V_2 w] dr \tag{36}$$

and

$$(k, N\Delta|G|k_0, NN) = 4\pi \int_0^{r_c} r j_{L'}(kr) F_{N\Delta}(r) dr + 4\pi r_c j_{L'}(kr_c) b^{-1} \left.\frac{dw}{dr}\right|_{r_c} + 4\pi \int_{r_c}^{\infty} r j_{L'}(kr)[V_3 w + V_2 u] dr \ . \tag{37}$$

Equations (28), (29), and (31)–(37) are the same as the tensor-coupled equations for the $NN$ system, except for the following differences:
In Eq. (29), for the nucleon-nucleon case, $b$ is replaced by unity, and $\gamma_2^2$ is replaced by $\gamma_0^2$. Also, in the nucleon-nucleon case $\varphi_{N\Delta}$ is replaced by $\varphi_{NN}$ on the right side of Eq. (35), and $b$ is replaced by unity in Eq. (37).

In the first iteration, Eqs. (28) and (29) are solved with $F_{NN} = F_{N\Delta} = 0$. Equations (36) and (37) are then used to obtain matrix elements of $G$, and these are inserted in Eqs. (34) and (35) to get improved estimates of $F_{NN}$ and $F_{N\Delta}$. These are put into the right sides of Eqs. (28) and (29), which are then solved again to begin the second iteration. This iteration procedure is continued until convergence is obtained. Only the diagonal matrix elements $(k_0, NN|G|k_0, NN)$ are used in calculating the binding energy.

The contribution from the channel with $N\Delta$ coupling to the defect parameter $\kappa$ may also be obtained. First we evaluate the defect integral

$$I = \left(k_0, NN\left|G\,\frac{Q}{e^2}\,G\right|k_0, NN\right) = I_{NN} + I_{N\Delta} \tag{38}$$

for a given initial state labeled by momenta $(k_0, P)$. The sum over intermediate states implied in Eq. (38) involves both $NN$ and $N\Delta$ states. The contributions from these two sets of intermediate states are called $I_{NN}$ and $I_{N\Delta}$, respectively. These quantities are evaluated by numerically evaluating the integrals

$$I_{NN} = (2\pi)^{-3} \int 4\pi k^2 dk \, \frac{(k, NN|G|k_0, NN)^2}{[e_{NN}(k, P)]^2} \, Q_{NN}(k, P) \tag{39}$$

and

$$I_{N\Delta} = (2\pi)^{-3} \int 4\pi k^2 dk \, \frac{(k, N\Delta|G|k_0, NN)^2}{[e_{N\Delta}(k, P)]^2} \, Q_{N\Delta}(k, P) \ . \tag{40}$$

The defect parameters $\kappa_{NN}$ and $\kappa_{N\Delta}$ are then given by

$$\kappa_{NN} = \nu\rho\bar{I}_{NN}, \quad \kappa_{N\Delta} = \nu\rho\bar{I}_{N\Delta} , \tag{41}$$

where $\bar{I}_{NN}$ and $\bar{I}_{N\Delta}$ are the respective averages of $I_{NN}$ and $I_{N\Delta}$ over occupied states $(k_0, P)$, $\rho$ is the density, and $\nu$ is the statistical weight

$$\nu = \tfrac{1}{8}(2J+1)(2T+1) \ . \tag{42}$$

The total contribution to $\kappa$ from the channel with $N\Delta$ coupling is the sum of $\kappa_{NN}$ and $\kappa_{N\Delta}$.

## V. NUCLEAR-MATTER CALCULATIONS

All our nuclear-matter calculations have been done in the following way:[1-3] The single-particle spectrum is made self-consistent for states in the Fermi sea and is taken to be pure kinetic energy for states above the sea. All two-body partial waves with $J \le 2$ are included, and channels with $J > 2$ are omitted. The energy per particle $\epsilon$ is

TABLE V. Energy per particle $\epsilon$ in MeV as a function of Fermi momentum $k_F$ for various two-body potentials. The labels of the potentials and the method of calculation are explained in the text. The numerical accuracy is about 0.03 MeV.

| Potential \ $k_F$ (fm$^{-1}$) | 1.2 | 1.3 | 1.36 | 1.4 | 1.5 | 1.6 | 1.7 | 1.8 |
|---|---|---|---|---|---|---|---|---|
| RSC | −10.04 | −11.04 | −11.44 | −11.59 | −11.50 | | | |
| RSC + Δ(S) | −7.74 | −7.83 | −7.61 | −7.32 | −6.01 | | | |
| RSC + Δ(S, $Q_{N\Delta}$ = 1) | −8.06 | −8.30 | −8.20 | −8.01 | −6.98 | | | |
| RSC + CORE(S) | −9.76 | −10.63 | −10.91 | −11.00 | −10.68 | | | |
| UG3 | | | −16.66 | | | −21.09 | −22.19 | −22.58 |
| UG3 + Δ(S) | −9.78 | −10.66 | −11.00 | −11.12 | −11.05 | | | |
| UG3 + 0.75Δ(S) | −10.65 | −11.86 | −12.43 | −12.72 | −13.10 | −12.83 | −11.78 | |
| RSC + Δ(P) | −9.28 | −9.90 | −9.96 | −9.87 | −9.05 | | | |
| RSC + Δ(P, $Q_{N\Delta}$ = 1) | −9.65 | −10.45 | −10.66 | −10.68 | −10.20 | | | |
| UG3 + Δ(P) | −12.50 | −14.18 | −15.05 | −15.53 | −16.40 | −16.56 | −15.87 | −14.10 |

then calculated in lowest-order Brueckner theory, i.e., including only two-body correlations.

Our first calculation uses the Reid soft-core potential[20] in all channels except $^1S_0$. In this channel the modified Haapakoski[25] potential with $N\Delta$ coupling is used, with the parameters given in column 2 of Table III. This calculation is labeled "RSC + Δ(S)." The calculated energies are shown in Table V as a function of $k_F$. The resulting saturation point is given in Table VI and is shown in Fig. 1. It is seen to lie in the saturation band.

Calculated values of the defect parameter $\kappa$ are shown in Table VII. The value $\kappa = 0.21$ for the RSC + Δ(S) potential is the same as that for the Hamada-Johnston[28] potential, which is seen from Fig. 1 to saturate at nearly the same point. Thus the usual correlation between the saturation point and the value of $\kappa$ persists when $N\Delta$ coupling is included in the $^1S_0$ state. The value of $\kappa$ for the RSC + Δ(S) calculation exceeds that of the Reid soft-core (RSC) calculation by 0.072. Of this increase 0.047 or 65% is seen to come directly from the $N\Delta$ channel, 0.016 or 22% comes from the $NN$ component of the $^1S_0$ channel, and 0.009 or 13% comes from other channels. In these other channels, the two-body potential is exactly the same in the two calculations, but the contribution to $\kappa$ is different because of the difference in the self-consistent single-particle spectrum.

Part of the increase in $\kappa$, and consequent loss of binding, in going from RSC to RSC + Δ(S) is due to the fact that the latter calculation uses a hard core of radius 0.4 fm in the $^1S_0$ state, while the RSC potential has a Yukawa core. To better isolate the effect of the $N\Delta$ coupling, a calculation

TABLE VI. Saturation points for various potentials.

| Potential | $k_F$ (fm$^{-1}$) | $\epsilon$ (MeV) |
|---|---|---|
| RSC | 1.44 | −11.64 |
| RSC + Δ(S) | 1.27 | −7.85 |
| RSC + Δ(S; $Q_{N\Delta}$ = 1) | 1.30 | −8.30 |
| RSC + CORE(S) | 1.41 | −11.00 |
| UG3 | 1.80 | −22.60 |
| UG3 + Δ(S) | 1.44 | −11.13 |
| UG3 + 0.75Δ(S) | 1.51 | −13.10 |
| RSC + Δ(P) | 1.35 | −9.96 |
| RSC + Δ(P, $Q_{N\Delta}$ = 1) | 1.39 | −10.68 |
| UG3 + Δ(P) | 1.57 | −16.60 |

TABLE VII. Contributions to $\kappa$ at $k_F = 1.36$ fm$^{-1}$. Column 1 specifies the two-body potential, as explained in the text. The second and third columns give the values of $\kappa_{NN}$ and $\kappa_{N\Delta}$, which are defined in Eqs. (39) through (42). The upper half of the table refers to calculations with the coupling $^1S_0(NN) \rightleftarrows {}^5D_0(N\Delta)$. Thus $\kappa_{NN}$ gives the contribution to $\kappa$ from the $^1S_0(NN)$ channel, $\kappa_{N\Delta}$ comes from the $^5D_0(N\Delta)$ channel, and "Sum" indicates the sum of these two. The column labeled "Other" gives the contribution from all other channels, and "Total" indicates the total contribution from all channels. Similarly, in the lower half of the table, $\kappa_{NN}$ corresponds to the $^3P_1(NN)$ channel and $\kappa_{N\Delta}$ to the $^5P_1(N\Delta)$ channel.

| | $\kappa_{NN}$ | $\kappa_{N\Delta}$ | Sum | Other | Total |
|---|---|---|---|---|---|
| Coupling $^1S_0(NN) \rightleftarrows {}^5D_0(N\Delta)$ | | | | | |
| RSC | 0.023 | ··· | 0.023 | 0.120 | 0.143 |
| RSC + Δ(S) | 0.039 | 0.047 | 0.086 | 0.129 | 0.215 |
| RSC + CORE(S) | 0.034 | ··· | 0.034 | 0.121 | 0.155 |
| UG3 | 0.012 | ··· | 0.012 | 0.062 | 0.074 |
| UG3 + Δ(S) | 0.039 | 0.045 | 0.084 | 0.070 | 0.154 |
| UG3 + 0.75Δ(S) | 0.037 | 0.027 | 0.064 | 0.068 | 0.132 |
| Coupling $^3P_1(NN) \rightleftarrows {}^5P_1(N\Delta)$ | | | | | |
| RSC | 0.0047 | ··· | 0.0047 | 0.138 | 0.143 |
| RSC + Δ(P) | 0.0086 | 0.0052 | 0.0138 | 0.141 | 0.155 |
| UG3 | 0.0036 | ··· | 0.0036 | 0.070 | 0.074 |
| UG3 + Δ(P) | 0.0078 | 0.0049 | 0.0127 | 0.072 | 0.085 |

was done using the Reid soft-core potential except that the $^1S_0$ potential was replaced by the potential given in column 5 of Table III, which has a hard core of radius 0.4 fm but no $N\Delta$ coupling. This calculation is labeled "RSC + CORE($S$)." The difference in $\kappa$ between this calculation and RSC + $\Delta(S)$ is 0.060, and only 0.005, or 8%, of this comes from the $^1S_0$ $NN$ channel. Thus the difference between the saturation points of RSC + $\Delta(S)$ and RSC + CORE($S$) is a reasonable measure of the effect of the coupling $^1S_0$ $(NN) \rightleftarrows {}^5D_0$ $(N\Delta)$. From Table VI we see that adding $N\Delta$ coupling to the RSC + CORE($S$) potential reduces the equilibrium binding energy and Fermi momentum by 3.15 MeV and 0.14 fm$^{-1}$, respectively.

As we discussed in the introduction, the $N\Delta$ coupling reduces the binding energy by two mechanisms: the dispersion effect and the Pauli effect. In order to separate these two effects, the RSC + $\Delta(S)$ calculation was repeated except that, when computing the $^1S_0$ reaction matrix, the Pauli operator $Q$ was replaced by unity in the $N\Delta$ channel. This calculation is labeled "RSC + $\Delta(S, Q_{N\Delta} = 1)$" and from Table VI it is seen that the results differ from RSC + $\Delta(S)$ by 0.45 MeV and 0.03 fm$^{-1}$ in energy and Fermi momentum, respectively. This difference is a measure of the Pauli effect, and it is only about 15% of the total change of 3.15 MeV and 0.14 fm$^{-1}$ in the saturation point caused by $N\Delta$ coupling. We attribute the rest of the effect to dispersion. Hence the effect of $N\Delta$ coupling in the $^1S_0$ state is about 85% due to dispersion and 15% due to the Pauli effect. The mechanism of the dispersion effect is discussed in detail in Sec. VI.

Since $N\Delta$ coupling reduces the binding energy and density, the question arises of whether adding this coupling to a potential that saturates at too high a binding energy and density can produce a saturation point lying in the empirical region shown in Fig. 1. To answer this question, a calculation was done using model 3 of the Ueda-Green (UG) one-boson-exchange potential,[21] except that the modified Haapakoski potential (column 2 of Table III) was used in the $^1S_0$ channel. This calculation is labeled UG3 + $\Delta(S)$, and the resulting saturation point is shown in Table VI and Fig. 1. It is shifted by 11.5 MeV from the ordinary Ueda-Green result (labeled UG3), but it still lies in the saturation band and is correlated with $\kappa$ in the usual way. Not all of the large difference in energy between UG3 and UG3 + $\Delta(S)$ can be attributed to $N\Delta$ coupling. Table VII shows that the difference in $\kappa$ in the $^1S_0$ channel is 0.072, but that only 0.045, or about 60%, of the difference comes from the $N\Delta$ channel. Thus only about 60% of the energy shift is caused by $N\Delta$ coupling.

As the coupling strength is reduced below $y = 1.0$, the saturation point for UG3 + $\Delta(S)$ will move along some path in Fig. 1 towards the region of higher density and higher binding energy. How close will the path come to the empirical region contained in the rectangular box? To answer this question, a similar calculation with $y = 0.75$ ($^1S_0$ potential from column 8 of Table III) was done. The results are labeled UG3 + 0.75$\Delta(S)$ and are shown in Fig. 1 and Tables V, VI, and VII. It appears that varying the coupling strength simply causes the saturation point to move along the saturation band and does not change the picture qualitatively.

The probability $P_\Delta$ that a particle in nuclear matter is a $\Delta$ rather than a nucleon is given by $\frac{1}{2}\kappa_{N\Delta}$. The contribution to $P_\Delta$ from the coupling $^1S_0$ $(NN) \rightleftarrows {}^5D_0$ $(N\Delta)$ is seen from Table VII to be about 2.3% in the RSC + $\Delta(S)$ calculation. The estimate of Green and Schucan[15] was 2.8%. The additional contributions to $P_\Delta$ from other $N\Delta$ couplings will be discussed later.

The Pauli term $\Delta\epsilon(P)$, the dispersion term $\Delta\epsilon(D)$, and the total energy shift $\Delta\epsilon = \Delta\epsilon(D) + \Delta\epsilon(P)$ are shown in Fig. 3 as functions of the density. They are well represented by straight lines on a logarithmic plot. The solid lines are obtained from the empirical formulas

$$\Delta\epsilon(D) = 0.926 k_F^{3.47}, \tag{43}$$

$$\Delta\epsilon(P) = 0.131 k_F^{4.94}, \tag{44}$$

and

$$\Delta\epsilon = 1.02 k_F^{3.76}. \tag{45}$$

Green and Niskanen[17] have also made estimates of the Pauli and dispersion effects for $N\Delta$ coupling in the $^1S_0$ channel of the Reid potential. Their results are compared with ours in Fig. 3. Detailed agreement is not expected between the two calculations for two reasons: (1) The form chosen for $V_2(r)$ is different in the two calculations, and (2) our results are obtained from a detailed Brueckner calculation, while Green and Niskanen have used approximate formulas of the type discussed in Sec. VI of this paper. We see from Fig. 3 that there is reasonable agreement between the two calculations for the dispersion effect. But we obtain a Pauli effect that is three to four times smaller than that of Green and Niskanen. The reason for this discrepancy is explained in Sec. VI A. The Green-Niskanen results are fitted by the empirical formulas

$$\Delta\epsilon(D) = 0.820 k_F^{4.31}, \tag{46}$$

$$\Delta\epsilon(P) = 0.336 k_F^{6.04}, \tag{47}$$

$$\Delta\epsilon = 0.702 k_F^{5.87}. \tag{48}$$

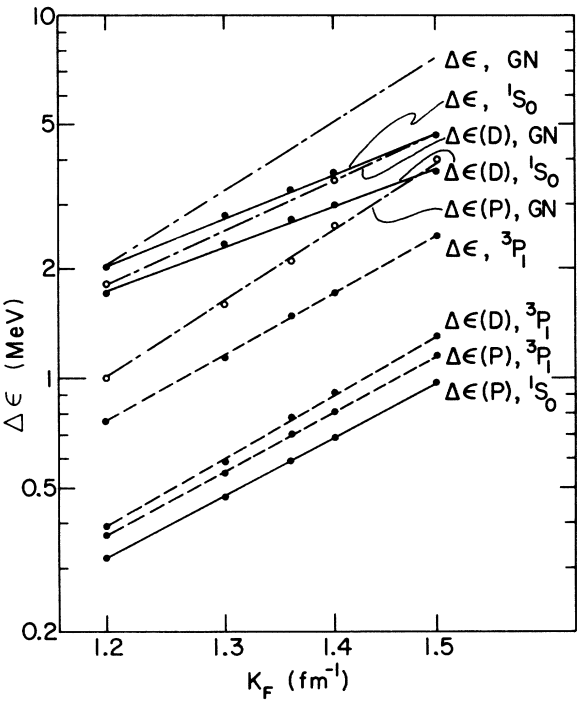


FIG. 3. Plot of energy shift vs Fermi momentum. Both scales are logarithmic, and $\Delta\epsilon(D)$, $\Delta\epsilon(P)$, and $\Delta\epsilon$ are the dispersion, Pauli, and total energy shifts, respectively. The solid circles give our calculated values. The solid and dashed lines show the empirical fits of Eqs. (43)–(45) and (49)–(51). The open circles are the values calculated by Green and Niskanen for $\Delta\epsilon(D)$ and $\Delta\epsilon(P)$. The dash-dot lines are empirical fits of Eqs. (46)–(48).

Green and Niskanen obtained Eq. (48) for $\Delta\epsilon$ by fitting their numerical results obtained from the lowest-order constrained variational (LOCV) method of Pandharipande.[29]

For the coupling $^3P_1$ $(NN) \rightleftarrows {}^5P_1$ $(N\Delta)$, we have calculated saturation curves in complete analogy to the $^1S_0$ case. The potential given in column 2 of Table IV is used in the $^3P_1$ channel, and in all other channels either the Reid of Ueda-Green potential is used. The results are shown in Figs. 1 and 3 and in Tables V, VI, and VII. The energy shifts are fitted by straight lines given by the expressions

$$\Delta\epsilon(D) = 0.146 k_F^{5.39}\,, \tag{49}$$

$$\Delta\epsilon(P) = 0.148 k_F^{5.05}\,, \tag{50}$$

and

$$\Delta\epsilon = 0.299 k_F^{5.21}\,. \tag{51}$$

The saturation points remain in the saturation band.

The difference in binding between the RSC and RSC + $\Delta(P)$ saturation points is 1.68 MeV, more than half as large as the effect of 3.15 MeV in the $^1S_0$ channel. From Table II, we see that there are several other nonnegligible $P$-wave couplings in addition to the coupling $^3P_1$ $(NN) \rightleftarrows {}^5P_1$ $(N\Delta)$ that we have chosen for detailed calculation. Thus the combined effect of all $P$-wave couplings may be comparable to that of the $S$-wave coupling.

For the coupling $^3P_1$ $(NN) \rightleftarrows {}^5P_1$ $(N\Delta)$, in contrast to the $^1S_0$ case, the Pauli effect of 0.72 MeV in energy and 0.04 $fm^{-1}$ in $k_F$ is comparable to the dispersion effect of 0.96 MeV and 0.05 $fm^{-1}$, respectively. Although the loss of binding is about half as large as in the $^1S_0$ case, the increase in $\kappa$ of 0.012 is only 17% of that in the $^1S_0$ case. The qualitative differences between $S$-wave and $P$-wave coupling are discussed further in the next section.

From Eqs. (45) and (51) we see that the energy shifts caused by $S$-wave and $P$-wave coupling vary with density as $k_F^{3.76}$ and $k_F^{5.21}$, respectively. These density dependences are not strong enough to move the saturation point off the saturation band. Thus it is of interest to determine how strong the density dependence must be to permit escape from the saturation band.

Suppose the calculated saturation point for some potential model occurs at a point $(\epsilon_0, k_{F0})$ in the saturation band. Inclusion of some new physical effect will give a new saturation point $(\epsilon_1, k_{F1})$, and whether or not we escape from the saturation band depends on the slope

$$S = (\epsilon_1 - \epsilon_0)/(k_{F1} - k_{F0}) \tag{52}$$

of the line joining the two saturation points. The new physical effect that is of interest for us is $N\Delta$ coupling. But the argument to be given below applies to any effect that gives some additional contribution to the energy, e.g., three-body forces, higher-order terms in the hole-line expansion, etc.

The value of the slope $S$ that is needed to escape the saturation band depends on whether the new physical effect increases or decreases the binding energy. For an effect that gives more binding, an escape from the saturation band in the desired direction might be accomplished by either a large negative slope or a positive slope. However, $N\Delta$ coupling always reduces both the equilibrium binding energy and density. Therefore, in order to escape from the saturation band through $N\Delta$ coupling, we must have $S$ much less negative than the slope of the saturation band. Near the empirical density, the slope of the saturation band is found from Fig. 1 to be about $-24$ MeV fm. A significant escape from the saturation band would

require $S$ to be much less negative than this, for instance $S=-15$ MeV fm.

We can estimate the density dependence required to give any desired value of $S$ as follows. Over the small interval of $k_F$ containing $k_{F1}$ and $k_{F0}$, we represent the energy shift due to the new effect by the function $\alpha k_F^n$, where $\alpha$ and $n$ are constants. The energy $\epsilon(k_F)$ without the new effect can be represented in this region by the first two terms of its Taylor expansion about $k_{F0}$. Thus we find for the energy $\epsilon'(k_F)$, which includes the new effect, the approximate formula

$$\epsilon'(k_F)=\epsilon_0+\frac{K}{2k_{F0}^2}(k_F-k_{F0})^2+\alpha k_F^n\,, \tag{53}$$

where the incompressibility parameter $K$ is defined by

$$K=k_{F0}^2\left.\frac{d^2\epsilon}{dk_F^2}\right|_{k_{F0}}. \tag{54}$$

The value of $k_{F1}$, which is obtained by minimizing formula (53), satisfies

$$\alpha k_{F1}^n+\frac{Kk_{F1}}{nk_{F0}^2}(k_{F1}-k_{F0})=0\,. \tag{55}$$

The saturation energy $\epsilon_1$ with the new effect is found by putting $k_F=k_{F1}$ in Eq. (53). Then, after using Eq. (55) to eliminate $\alpha$, we easily evaluate Eq. (52) to get

$$S=-\frac{K}{nk_{F0}}-\frac{K}{2k_{F0}^2}\left(1-\frac{2}{n}\right)(k_{F0}-k_{F1})\,. \tag{56}$$

For the RSC potential we have[14] $K\approx 150$ MeV, $k_{F0}=1.44$ fm$^{-1}$, and putting these values into Eq. (56) gives

$$S=-\frac{104}{n}-36\left(1-\frac{2}{n}\right)(k_{F0}-k_{F1})\,. \tag{57}$$

In this equation, $S$ is given in MeV fm when $k_{F1}$ and $k_{F0}$ are given in fm$^{-1}$.

We have seen that in order to move appreciably out of the saturation band through $N\Delta$ coupling, we must have $|S|$ no larger than about 15 MeV fm. Using Eq. (57), we can estimate the value of $n$ needed to accomplish this. Since $N\Delta$ coupling reduces the saturation density, the second term of Eq. (57) is negative and therefore gives a positive contribution to $|S|$. Thus minimizing $|S|$ means minimizing this term, which means making the density shift zero. However, in order to move significantly out of the saturation band by means of a small negative slope $S$, we must clearly have a density shift that is not too small, say $k_{F0}-k_{F1}\geq 0.1$ fm$^{-1}$. Imposing this requirement, we see from Eq. (57) that we must have $n\gtrsim 8.5$ in order that $|S|$ be smaller than 15 MeV fm. We conclude that, if we are to escape the saturation band, the density dependence of the energy shift due to $N\Delta$ coupling must be $k_F^{8.5}$ or stronger. This is a much stronger density dependence than we have found for either $S$-wave or $P$-wave coupling.

## VI. APPROXIMATIONS AND QUALITATIVE UNDERSTANDING

In this section we derive approximate formulas and use them to understand the main features of the previous results. In Sec. VI A we derive the necessary formulas and test them by comparison with the results obtained in Sec. V. The difference in $\Delta\epsilon(P)$ between our work and that of Green and Niskanen[17] is readily explained by these formulas. In Sec. VI B we discuss the qualitative differences between $S$-wave and $P$-wave coupling and study the density dependence of $\Delta\epsilon$, which determines whether or not we might escape from the saturation band. In Sec. VI C we estimate the effect of $N\Delta$ couplings not treated by detailed calculation.

### A. Approximate formulas

We start with the relation between $G$ matrices calculated with different propagators $X$. This approach has often been used before, in particular by Green and Niskanen.[17] If $G_\alpha$ satisfies

$$G_\alpha=V-VX_\alpha G_\alpha\,, \tag{58}$$

with a similar equation for $G_\beta$, we have[30]

$$G_\alpha-G_\beta=G_\beta(X_\beta-X_\alpha)G_\alpha\,. \tag{59}$$

We consider the coupled $NN$ and $N\Delta$ channels and distinguish among three different nuclear-matter propagators $X$. In all three cases, the $NN$ part of the propagator is chosen to be $(Q_{NN}/e_{NN})$, as is appropriate for nuclear matter. But in the $N\Delta$ channel we consider

$$X_{N\Delta}^A=\frac{1}{e_0}\,, \tag{60}$$

where

$$e_0=T+(\Delta-M)c^2-T_i-T_j\,,$$

and

$$X_{N\Delta}^B=\frac{1}{e}\,, \tag{61}$$

where

$$e=e_0-U_i-U_j\,,$$

and

$$X_{N\Delta}=Q_{N\Delta}/e\,. \tag{62}$$

Here $T$ is the two-body kinetic-energy operator, and $T_i$ and $T_j$ ($U_i$ and $U_j$) are the kinetic (po-

tential) energies of the two nucleons in the Fermi sea.

The propagator $X^A_{N\Delta}$ is appropriate for scattering. Using it in nuclear matter neglects both Pauli and dispersion effects and corresponds to a nuclear-matter calculation with an ordinary potential such as that of Reid or Ueda and Green. The propagator $X^B_{N\Delta}$ has been used in our calculations with $Q_{N\Delta}=1$ and includes the dispersion effect but not the Pauli effect. Finally, $X_{N\Delta}$ is the correct nuclear-matter propagator that includes both effects.

The binding energy depends on diagonal matrix elements $\langle NN|G|NN\rangle$ in the $NN$ channel (the other labels of the state $|NN\rangle$ have been suppressed). The change $\Delta G(D)$ in this matrix element due to dispersion is found from Eqs. (59), (60), and (61) to be

$$\Delta G(D)=\langle NN|G_B-G_A|NN\rangle$$

$$=\left\langle NN\left|G_{2A}\frac{e-e_0}{e_0e}G_{2B}\right|NN\right\rangle, \tag{63}$$

where the subscript 2 on $G$ indicates that part of $G$ that connects the $NN$ and $N\Delta$ channels. Similarly, the change due to the Pauli effect is

$$\Delta G(P)=\langle NN|G-G_B|NN\rangle$$

$$=\left\langle NN\left|G_{2B}\frac{1-Q_{N\Delta}}{e}G_2\right|NN\right\rangle. \tag{64}$$

These formulas could be evaluated exactly by computing the required $G$-matrix elements and integrating over the relative momentum $k$ of intermediate states. However, we are interested at the moment in obtaining insight into our results rather than in high numerical accuracy. For this purpose, it is often convenient to approximate one or more of $G_A$, $G_B$, and $G$ by another of these that is more easily calculated.

How much error does this replacement cause? We first note that the difference between $G_B$ and $G$ comes from the difference between $Q_{N\Delta}$ and unity. But $Q_{N\Delta}$ excludes a sphere of radius $k_F$ in $k$ space, while relative momenta $k$ as large as 3–4 fm$^{-1}$ are known to be important for the calculation of $G$. Thus, $Q_{N\Delta}$ differs from unity in only a fraction $(k_F/3\text{ fm}^{-1})^3\approx 10\%$ of the relevant region of phase space. Second, the difference $G_B-G_A$ comes from the difference $e-e_0=-(U_i+U_j)$, which is typically 135 MeV. But for an intermediate state with a typical relative momentum $k$ of 3 fm$^{-1}$, $e$ is about 700 MeV. Thus, changing $e$ to $e_0$ changes the propagator by about 20%. Finally, the propagators for $G_A$, $G_B$, and $G$ differ only in the $N\Delta$ channel, not in the $NN$ channel. So we expect the approximation $G_A\approx G_B\approx G$ to be good to roughly 25%, and this is sufficient for our present purpose.

The procedure used by Green and co-workers[15-17] emerges from this treatment if all the $G_2$'s in Eqs. (63) and (64) are approximated by $G_{2A}$, and, in addition, $V_3$ is neglected. The neglect of $V_3$ is reasonable because it always occurs added to the much larger $N\Delta$ mass difference of 300 MeV [see Eqs. (3), (25), and (29)]. Also, Green and Haapakoski[16] have verified numerically that neglecting $V_3$ has a small effect on the $^1S_0$ phase shifts. The matrix elements needed to evaluate formulas (63) and (64) are then

$$\langle k,N\Delta|G_{2A}|NN\rangle=\langle k,N\Delta|V_2|\psi_A\rangle\ , \tag{65}$$

where $\psi_A$ is the correlated two-body wave function corresponding to the propagator $X_A$, and $k$ is the relative momentum of the intermediate $N\Delta$ state. Now, $\psi_A$ has both a $NN$ and a $N\Delta$ component. But, since $V_2$ connects only the $NN$ and $N\Delta$ channels, only the $NN$ component of $\psi_A$ is needed in expression (65). The propagator $X_A$, which omits both the Pauli and dispersion effects in the $N\Delta$ channel, corresponds to a calculation with an ordinary potential, such as that of Reid, that has no $N\Delta$ coupling. Thus the $NN$ component of $\psi_A$ must be identified with the usual Bethe-Goldstone wave function $\psi_{BG}$, calculated with an ordinary potential without $N\Delta$ coupling. If $\psi_{BG}$ is available, the effects of $N\Delta$ coupling can thus be estimated quite simply. Green and co-workers[15-17] have obtained useful results by this procedure. It has the virtue of avoiding both the fitting of $NN$ phases with coupled-channel potentials and the calculation of the nuclear-matter $G$ matrix with these potentials.

Our first aim is to check this type of approximation by comparison with the results of the last section. Then we can use the approximate formulas to gain a better understanding of the results. In our computations, the most readily available $G$ matrix is calculated with the full nuclear-matter propagator $X$ of Eq. (62). We therefore find it convenient to estimate expressions (63) and (64) by approximating $G_{2A}$ and $G_{2B}$ by $G_2$. Using $e-e_0=-(U_i+U_j)$, we then rewrite Eq. (63) in the form

$$\Delta G(D)=-(U_i+U_j)$$

$$\times\left\langle NN\left|G_2\left[\frac{Q_{N\Delta}}{e_0e}G_2+\frac{1-Q_{N\Delta}}{e_0e}G_2\right]\right|NN\right\rangle. \tag{66}$$

In Eq. (66) we have somewhat artificially split the term $(e_0e)^{-1}$ from Eq. (63) into two terms. This will allow us to relate the dispersion term to $\kappa_{N\Delta}$, which is useful in understanding why the energy shift for $S$-wave coupling is so closely correlated

with $\kappa_{N\Delta}$.

In the first term of Eq. (66) we replace $e_0$ by $e$, which should be accurate to about 20%, as explained above. In the second term, only small relative momenta occur because of the factor $1 - Q_{N\Delta}$. The kinetic-energy terms in $e_0$ are then small, and in addition they tend to cancel. So it is sufficiently accurate to replace $e_0$ by $(\Delta - M)c^2$ in the second term of Eq. (66).

With these approximations, formulas (66) and (64) become

$$\Delta G(D) = -(U_i + U_j)[I_{N\Delta} + I_P] , \tag{67}$$

$$\Delta G(P) = (\Delta - M)c^2 I_P , \tag{68}$$

where

$$I_{N\Delta} = \int \frac{d^3k}{(2\pi)^3} \frac{\langle k, N\Delta | G | NN\rangle^2}{[e(k)]^2} Q_{N\Delta}(k) \tag{69}$$

is the contribution to the defect integral from the $N\Delta$ channel, and

$$I_P = \int \frac{d^3k}{(2\pi)^3} \frac{\langle k, N\Delta | G | NN\rangle^2}{(\Delta - M)c^2 e(k)} [1 - Q_{N\Delta}(k)] \tag{70}$$

is a corresponding "Pauli" defect integral. It appears in the dispersion effect because we have analyzed $\Delta G(D)$ in terms of the exact defect integral $I_{N\Delta}$ that is calculated with the correct Pauli operator $Q_{N\Delta}$.

Having $\Delta G$, we obtain the corresponding change $\Delta\epsilon$ in the energy by averaging over initial states in the Fermi sea and multiplying by $\frac{1}{2}\rho\nu$, where $\rho$ is the density, and the statistical weight $\nu$ of the channel is given by Eq. (42). Since $U(k)$ typically varies by only 25% as $k$ varies from 0 to $k_F$, we replace $(U_i + U_j)$ in Eq. (67) by its average value $2\bar{U}$. Then we get

$$\Delta\epsilon(D) = -\bar{U}[\kappa_{N\Delta} + \kappa_P] , \tag{71}$$

where

$$\kappa_{N\Delta} = \rho\nu\bar{I}_{N\Delta}, \quad \kappa_P = \rho\nu\bar{I}_P , \tag{72}$$

and the bar over $I_{N\Delta}$ or $I_P$ indicates an average over initial two-particle states in the Fermi sea. Similarly, we find for the Pauli effect the result

$$\Delta\epsilon(P) = \tfrac{1}{2}(\Delta - M)c^2\kappa_P . \tag{73}$$

Formulas (71) and (73) are applicable when the same single-particle spectrum is used with $N\Delta$ coupling as without it. However, in self-consistent calculations, the spectrum of occupied states will change when $N\Delta$ coupling is added. If the single-particle potential of each occupied state is changed by $\Delta U$, this causes a change in $\epsilon$ of $-\kappa\Delta U$, where $\kappa$ is the *total* defect parameter, summed over all partial waves. Thus the total change in energy, when $N\Delta$ coupling is included, is

$$\Delta\epsilon = \Delta\epsilon(D) + \Delta\epsilon(P) - \kappa\Delta U . \tag{74}$$

However, the self-consistency condition implies

$$\Delta U = 2\Delta\epsilon . \tag{75}$$

Eliminating $\Delta U$ from the last two equations gives

$$\Delta\epsilon = (1 + 2\kappa)^{-1}[\Delta\epsilon(D) + \Delta\epsilon(P)] . \tag{76}$$

This gives the energy difference caused by $N\Delta$ coupling between two *self-consistent* calculations.

Therefore the approximations (71) and (73), divided by $1 + 2\kappa$, are compared with our accurate numerical results. However, we expect that evaluating Eqs. (63) and (64) by using the approximation (65), with $\psi_A \to \psi_{BG}$, will be of comparable accuracy. This latter procedure is much more convenient when coupled-channel calculations for both scattering and nuclear matter are not readily available.

To test the approximate formulas, we compare them with our numerical results at $k_F = 1.36$ fm$^{-1}$ for $N\Delta$ coupling added to the Reid potential. We use $(\Delta - M)c^2 = 300$ MeV, $\bar{U} = -68$ MeV, and we obtain values of $1 + 2\kappa$ from Table VII.

We consider first the coupling ${}^1S_0(NN) \rightleftharpoons {}^5D_0(N\Delta)$. For the RSC + $\Delta(S)$ calculation, we have $\kappa_{N\Delta} = 0.047$ from Table VII. In evaluating $\kappa_P$, the average over initial states in the Fermi sea was approximated by using a single initial state with relative momentum $(3/10)^{1/2}k_F = 0.745$ fm$^{-1}$. The result is $\kappa_P = 0.0049$, about 10 times smaller than $\kappa_{N\Delta}$. The dispersion effect is the difference between the calculations labeled RSC + CORE($S$) and RSC + $\Delta(S, Q_{N\Delta} = 1)$. The average total $\kappa$ for these is 0.185. Dividing formula (71) by $1 + 2\kappa$ then gives $\Delta\epsilon(D) = 2.60$ MeV, which agrees well with the value 2.71 MeV obtained from the detailed calculations of Table V. The Pauli effect is the difference between the RSC + $\Delta(S)$ and the RSC + $\Delta(S, Q_{N\Delta} = 1)$ results. Taking $\kappa = 0.215$, we divide Eq. (73) by $1 + 2\kappa$ to get $\Delta\epsilon(P) = 0.51$ MeV, in good agreement with the value 0.59 MeV obtained from Table V. Thus the approximate formulas work well for $S$-wave coupling.

Before testing the approximate formulas for $P$-wave coupling, we discuss the large difference seen in Fig. 3 between our value of $\Delta\epsilon(P)$ for $S$-wave coupling and that of Green and Niskanen.[17] The values of $\Delta\epsilon(P)$ used by Green and Niskanen are taken from Green and Schucan.[15] Their calculations are based on the methods described in this section. However, Green and Schucan assumed that $I_P$ could be averaged over initial two-body states in the Fermi sea by calculating a single value with initial relative momentum $k_0 = 0$. When $V_3$ is neglected, as was shown above to be reasonable, the matrix element appearing in Eq. (70) for $I_P$ is

$$\langle k, N\Delta | G | NN \rangle = 4\pi \int r j_{L'}(kr) V_2(r) u_L(k_0, r) dr \ , \quad (77)$$

where $u_L(k_0, r)$ is the $NN$ wave function. For the coupling ${}^1S_0(NN) \rightleftarrows {}^5D_0(N\Delta)$, we have $L' = 2$ and $L = 0$. Since only small $k$ are relevant for $I_P$, the factor $j_2(kr)$ in Eq. (77) will rise rapidly as $r$ increases. Thus large values of $r$, where $u_0(k_0, r)$ is approximately equal to $rj_0(k_0 r)$, will contribute appreciably. When $k_0 = 0$, we have $u_0 \approx r$ in this region, but for $k_0 \sim \frac{1}{2}k_F$, say, we have $u_0 \approx k_0^{-1} \sin k_0 r$, which is much smaller than $r$ for $r \gtrsim 1.5$ fm. Thus the value of $I_P$ will be much larger for $k_0 = 0$ than for the average value of $k_0$ that we have used. Using $k_0 = 0$, we have repeated our calculation of $\kappa_P$, obtaining the value 0.0120, which is 2.5 times larger than the value obtained with $k_0 = 0.745$ fm$^{-1}$. This accounts for a factor 2.5 between our values of $\Delta\epsilon(P)$ and those quoted by Green and Niskanen. An additional factor of 1.5 comes from their use of $(f^{*2}/4\pi) = 0.35$ for the $\pi N\Delta$ coupling constant, while Haapakoski,[25] whose potential we use, chose the value 0.23. Together, these factors account satisfactorily for the large difference in Pauli effects shown in Fig. 3.

Turning to the ${}^3P_1$ case, we have $\kappa_{N\Delta} = 0.0052$ from Table VII. An accurate average of $I_P$ over the Fermi sea gives the result $\kappa_P = 0.0062$. Equations (71) and (73), renormalized by the appropriate values of $1 + 2\kappa$, then give values of 0.60 and 0.72 MeV for $\Delta\epsilon(D)$ and $\Delta\epsilon(P)$, respectively. These are reasonably close to the values of 0.78 and 0.70 that can be read from Table V for $k_F = 1.36$ fm$^{-1}$. Thus the approximate formulas are also sufficiently reliable for $P$-wave coupling.

### B. Qualitative interpretation

Having verified that the approximate formulas work well, we use them to gain insight into the numerical results. Consider first the relative size of the dispersion and Pauli effects, which was found in Sec. V to be so different for $S$-wave and $P$-wave coupling. This is seen from Eqs. (69) and (70) to depend on the behavior of $\langle k, N\Delta | G | k_0, NN \rangle$ as a function of $k$. If we neglect $V_3$ as before, this matrix element is given by Eq. (77). For the coupling ${}^1S_0(NN) \rightleftarrows {}^5D_0(N\Delta)$, the $N\Delta$ state has $L' = 2$, and, for values of $r$ within the range of $V_2(r)$, the factor $j_2(kr)$ in Eq. (77) becomes large only for large $k$. However, according to Eqs. (69) and (70), only small values of $k$ can contribute to the integral $I_P$, while large values contribute to $I_{N\Delta}$. It is therefore plausible that $I_P$ is much smaller than $I_{N\Delta}$ and hence $\Delta\epsilon(P) \ll \Delta\epsilon(D)$. The importance of the value of $L'$ for the behavior of $\langle k, L', N\Delta | G | k_0, L, NN \rangle$ has been emphasized by Bodmer and Rote.[18]

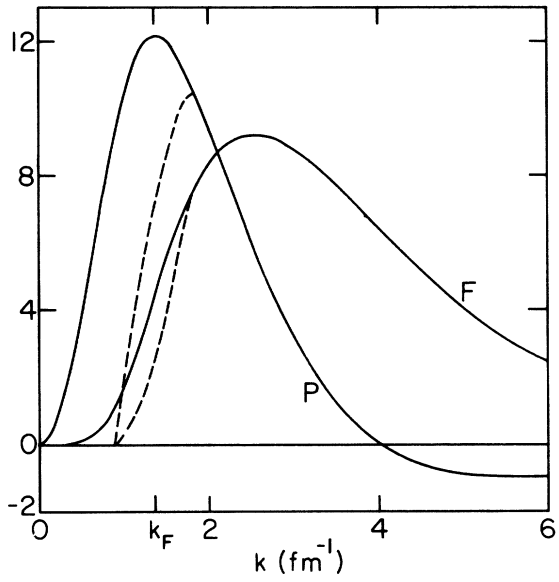


FIG. 4. The dimensionless quantity $k\langle k, L', N\Delta | G | k_0, L = 1, NN \rangle$ (defined by Eq. (37)) vs $k$. The curves labeled $P$ and $F$ correspond to $L' = 1$ and 3, respectively. Multiplying by $Q_{N\Delta}(k, P)$ results in the dashed curves. For $k < 0.9$ fm$^{-1}$, the dashed curves have the value zero, while for $k > 1.8$ fm$^{-1}$, they coincide with the corresponding solid lines. The values of other parameters used are $k_F = 1.36$ fm$^{-1}$, $k_0 = 1.02$ fm$^{-1}$, $P = 1.09$ fm$^{-1}$, $\gamma^2 = 2.02$ fm$^{-2}$, $\gamma_2^2 = 10.39$ fm$^{-2}$. The interaction is that for the coupling ${}^3P_1(NN) \rightleftarrows {}^5P_1(N\Delta)$ with $y = 1$ (column 2 of Table IV).

The same ideas can be applied to $P$-wave coupling, for which $L' = 1$ or 3. For $L' = 3$, we expect the Pauli effect to be negligible compared to the dispersion effect. But for $L' = 1$, the ratio of Pauli to dispersion effects should be larger than the value 1:5 obtained for the coupling ${}^1S_0(NN) \rightleftarrows {}^5D_0(N\Delta)$. Indeed, the calculations presented in Sec. V showed that the two effects are comparable for the coupling ${}^3P_1(NN) \rightleftarrows {}^5P_1(N\Delta)$. These ideas are illustrated in Fig. 4, where $k\langle k, L', N\Delta | G | k_0, L = 1, NN \rangle$ is plotted against $k$ for $L' = 1$ and $L' = 3$. When this quantity is multiplied by $Q_{N\Delta}(k, P)$, the dashed lines are obtained (to the left of the dashed lines we have $Q_{N\Delta} = 0$, and to the right, $Q_{N\Delta} = 1$). This figure, taken together with Eqs. (69) and (70), shows clearly that $I_P \ll I_{N\Delta}$ for $L' = 3$. The approximate equality of $I_P$ and $I_{N\Delta}$ for $L' = 1$ is also understandable from the figure.

Thus the value of $L'$ in the $N\Delta$ channel accounts for the relative size of $\kappa_P$ and $\kappa_{N\Delta}$ in different channels. The dependence of the energy shifts on $\kappa_{N\Delta}$ and $\kappa_P$ is given by Eqs. (71) and (73). For $S$-wave couplings $\kappa_P$ is negligible, while for $P$-wave coupling it is comparable to $\kappa_{N\Delta}$. The $\kappa_P$

contribution explains the different behavior of $S$- and $P$-wave couplings we observed in Sec. V.

The density dependence of our results can also be understood from the approximate formulas. Consider first the dispersion effect. As explained in Sec. VI A, we may put $\psi_A = \psi_{BG}$ in Eq. (65) and $e - e_0 = -2\bar{U}$ in Eq. (63). Then Eq. (63) becomes

$$\Delta G(D) = -2\bar{U}\left\langle \psi_{BG}\left| V_2 \frac{1}{e_0 e} V_2 \right| \psi_{BG}\right\rangle . \tag{78}$$

For qualitative considerations, it is reasonable to make a closure approximation in which $e_0$ and $e$ are replaced by appropriate average values $\bar{e}_0$ and $\bar{e}$, respectively. We expect these average values to be 500–700 MeV. They are both at least as large as the $\Delta N$ mass difference of 300 MeV. This leads to

$$\Delta G(D) \approx -\frac{2\bar{U}}{\bar{e}_0 \bar{e}} 4\pi \int dr [u_L(k_0, r)]^2 [V_2(r)]^2 , \tag{79}$$

where $u_L(k_0, r)$ is $r$ times the Bethe-Goldstone wave function for relative momentum $k_0$.

The energy shift $\Delta\epsilon(D)$ is obtained by averaging Eq. (79) for $\Delta G(D)$ over relative momenta $k_0$ in the Fermi sea and multiplying by $\frac{1}{2}\nu\rho(1+2\kappa)^{-1}$. We now consider the density dependence of $\Delta\epsilon(D)$. The density $\rho$ is proportional to $k_F^3$, and, since $\kappa \ll 1$, we may neglect the density dependence of $(1+2\kappa)^{-1}$. Considering next the factor $(\bar{e}_0\bar{e})^{-1}$ in Eq. (79), we note that the density dependence of $\bar{e} = e_0 - 2\bar{U}$ comes mainly from the density dependence of $\bar{U}$. But, since $\bar{e}$ is 4 to 6 times as large as $-2\bar{U}$, the density dependence of $\bar{e}$ is much weaker than that of $-2\bar{U}$. And $\bar{e}_0$ has a still weaker density dependence than $\bar{e}$. Therefore, in Eq. (79), the density dependence of the coefficient to the left of the integral comes mostly from the numerator $-2\bar{U}$, and the weaker density dependence of the denominator $\bar{e}_0\bar{e}$ can be neglected. Near the empirical density, our calculations show that $\bar{U}$ varies roughly as $k_F^{1.5}$ for the RSC potential.

The remaining density dependence of $\Delta\epsilon(D)$ comes from the integral in Eq. (79), averaged over relative momenta $k_0$ in the Fermi sea. This averaging may be approximated by using a single average relative momentum $\bar{k}_0$, which we assume to vary linearly with $k_F$. Putting these results together, we find the density dependence of $\Delta\epsilon(D)$ to be roughly

$$\Delta\epsilon(D) \propto k_F^{4.5} F_1 , \tag{80}$$

where

$$F_1 = \int [u_L(\bar{k}_0, r)]^2 [V_2(r)]^2 dr . \tag{81}$$

It remains to estimate the density dependence of $F_1$. This can be done by using our knowledge of the qualitative behavior of $u_L$. For a potential, such as RSC, with a strong short-range repulsion, $u_L$ is small inside about 0.5 fm and is not very different from the unperturbed wave function $rj_L(k_0 r)$ over most of the region outside this. Hence a reasonable estimate of $F_1$ is

$$F_1 \approx \int_{r_0}^{\infty} [rj_L(\bar{k}_0 r)]^2 [V_2(r)]^2 dr , \tag{82}$$

where $r_0 = 0.5$ fm.

We have not found any simple analytical way to estimate the dependence of expression (82) on $\bar{k}_0$. So we have evaluated Eq. (82) numerically, using the form $Y(0.7r)$ from Eq. (18) for $V_2(r)$. This form agrees with the static limit of meson theory at large $r$ and has an $r^{-1}$ singularity at small $r$. We have evaluated Eq. (82) for $L = 0, 1, 2, 3$, and for values of $\bar{k}_0$ in the range 0.6–1.2 fm$^{-1}$. This range of $\bar{k}_0$ should be reasonable when $k_F$ is near the empirical value of 1.36 fm$^{-1}$. The calculated values of $F_1$ are found to vary with $\bar{k}_0$ according to the formula

$$F_1 \propto \bar{k}_0^{1.5L-0.3} , \tag{83}$$

where the exponent of $\bar{k}_0$ is uncertain by about 0.5. This is not serious because, with our rough approximations, we only hope to get the exponent of $k_F$ correct to within one or two units.

Since $\bar{k}_0$ is linear in $k_F$, the power law of Eq. (83) also gives the dependence of $F_1$ on $k_F$. Our estimate for the density dependence of $\Delta\epsilon(D)$ is thus found from Eqs. (80) and (83) to be

$$\Delta\epsilon(D) \propto k_F^{4.2+1.5L} . \tag{84}$$

The density dependence of $\Delta\epsilon(D)$ depends on the orbital angular momentum $L$ of the $NN$ channel but not on its value $L'$ in the $N\Delta$ channel, and the density dependence is stronger for larger $L$. For $S$-wave and $P$-wave couplings, Eq. (84) predicts $\Delta\epsilon(D)$ to vary as $k_F^{4.2}$ and $k_F^{5.7}$, respectively. This should be compared to the density dependence given by Eqs. (43) and (49). Figure 5 shows the comparison for the interesting range of $k_F$. For this range the agreement is satisfactory.

We next estimate the density dependence of the Pauli term $\Delta\epsilon(P)$, which is proportional to $k_F^3 I_P$, where $I_P$ is defined by Eq. (70). We must average $I_P$ over the relative momentum $k_0$ of the initial $NN$ state in the Fermi sea. As before, we approximate this averaging by using a single average value $\bar{k}_0$, assuming it to vary linearly with $k_F$. Because of the factor $1 - Q_{N\Delta}(k)$ in Eq. (70), the relative momentum $k$ of the $N\Delta$ state is also restricted to low values, mainly those in the Fermi sea. So we make the rough approximation

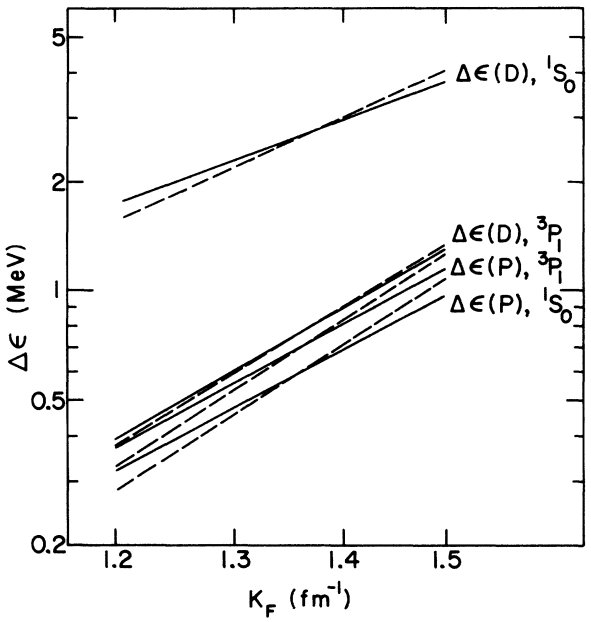


FIG. 5. Comparison of density dependence obtained from the approximate formulas (84) and (90) with the numerical results of Sec. V. Both scales are logarithmic. The solid lines are the empirical fits of Eqs. (43)–(44) and (49)–(50). The dashed lines are the predictions of the approximate formulas (84) and (90). Each dashed line is normalized to coincide with the corresponding solid line at $k_F = 1.36$ fm$^{-1}$.

$$I_P \approx \frac{\langle \bar{k}_0, N\Delta | G_2 | \bar{k}_0, NN\rangle^2}{(\Delta - M)c^2 e(\bar{k}_0)} \int \frac{d^3k}{(2\pi)^3} [1 - Q_{N\Delta}(k)] . \tag{85}$$

Here, in $e(k)$ and in the matrix element of $G_2$, we have replaced $k$ by an average value, which we take to be $\bar{k}_0$. Just as in the dispersion term, the density dependence of $e(\bar{k}_0)$ can be neglected. The integral in Eq. (85) is

$$\int d^3k[1 - Q_{N\Delta}(k)] = \tfrac{4}{3}\pi k_F^3 . \tag{86}$$

Using these results, along with Eq. (77) for $\langle \bar{k}_0, N\Delta | G_2 | \bar{k}_0, NN\rangle$, we obtain for the density dependence of $\Delta\epsilon(P)$ the estimate

$$\Delta\epsilon(P) \propto k_F^6 F_2^2 , \tag{87}$$

where

$$F_2 = \int r j_{L'}(\bar{k}_0 r) V_2(r) u_L(\bar{k}_0, r) dr . \tag{88}$$

Following our earlier treatment of $F_1$, we estimate $F_2$ numerically by putting $u_L(\bar{k}_0, r) = r j_L(\bar{k}_0 r)$ and integrating over the region $r > 0.5$ fm. Using again Eq. (18) for the form of $V_2(r)$, we find that the numerical results are roughly fitted, for $0.6 \text{ fm}^{-1} \leq k_0 \leq 1.2 \text{ fm}^{-1}$ by

$$F_2 \propto \bar{k}_0^{(1/2)(L'+L)-1} . \tag{89}$$

The uncertainty in the exponent is about 0.5. Combining Eqs. (87) and (89) gives

$$\Delta\epsilon(P) \propto k_F^{4+L+L'} . \tag{90}$$

For the couplings $^1S_0(NN) \rightleftharpoons {}^5D_0(N\Delta)$ and $^3P_1(NN) \rightleftharpoons {}^5P_1(N\Delta)$, Eq. (90) predicts $\Delta\epsilon(P)$ to vary as $k_F^6$ in both cases. The detailed calculations give density dependences of $k_F^{4.94}$ and $k_F^{5.05}$, respectively [see Eqs. (44) and (50)]. Figure 5 shows how well Eq. (90) fits the computed results over a limited range of $k_F$. Considering the roughness of our approximations, the agreement is satisfactory.

Equations (84) and (90) give us a good idea of how $\Delta\epsilon(D)$ and $\Delta\epsilon(P)$ vary with $k_F$. We see that the density dependence of $\Delta\epsilon(D)$ depends only on $L$, while that of $\Delta\epsilon(P)$ depends on both $L$ and $L'$. The density dependence becomes stronger for larger values of $L$ and $L'$.

The density dependence is very important because it determines whether $N\Delta$ coupling will allow us to escape from the saturation band, which is the main question that we want to answer. To provide a general answer to this question, we must determine the sensitivity of the estimates (84) and (90) to our assumptions about the two-body interaction. The assumptions concerning the potentials that we have made are (1) the potential $V_1$ has a strong short-range repulsion, and (2) the form of $V_2(r)$ is that of Eq. (18). Let us consider whether different assumptions would lead to a different density dependence.

We consider first the case when our assumption of a strong short-range repulsion in the $NN \rightleftharpoons NN$ potential $V_1$ is not valid. Suppose that there is no short-range repulsion at all. Then we may approximate $u_L(\bar{k}_0, r)$ by $r j_L(\bar{k}_0 r)$ for all $r$, and $F_1$ and $F_2$ are estimated by integrating over *all* $r$ in Eqs. (82) and (88), not only over the region $r > 0.5$ fm. We have done these integrals numerically, and we find that the estimates of Eqs. (83) and (89) for the behavior of $F_1$ and $F_2$ are practically unchanged. This is easy to understand. For $L = 0$ in $F_1$, and for $L = L' = 0$ in $F_2$, these quantities are seen, from Eqs. (83) and (89), to vary rather slowly with $\bar{k}_0$ when we integrate over $r > 0.5$ fm. But the contribution to either integral from $r < 0.5$ fm depends on $\bar{k}_0$ through the factor $j_0^2(\bar{k}_0 r)$, which, for small $r$, also varies slowly with $\bar{k}_0$. Thus the new contribution from $r < 0.5$ fm varies with $\bar{k}_0$ in about the same way as the contribution from $r > 0.5$ fm, and adding the new contribution does not change the density dependence. If $L \geq 1$ in $F_1$, or if $L + L' \geq 2$ in $F_2$, the

integrand of either integral is small for small $r$, and the contribution from $r \leq 0.5$ fm is unimportant. Hence this contribution does not change the density dependence of $F_1$ or $F_2$. We conclude that our estimates of density dependence are insensitive to the presence or absence of a strong short-range repulsion.

It is interesting to note that, although a short-range repulsion has little effect on the density dependence, it has a large effect on the *size* of $\Delta\epsilon(D)$ for $L=0$. Evaluating Eq. (82) for $r_0=0$ gives a result about 5 times as large as for $r_0=0.5$ fm. A similar sensitivity to short-range correlation has been found in calculations of the amount of $\Delta\Delta$ component in the deuteron.[31] For $L \geq 1$ in $F_1$, or for $L+L' \geq 2$ in $F_2$, the region $r \leq 0.5$ fm is relatively unimportant, and we expect the size of the energy shift to be insensitive to short-range correlations.

We next consider the sensitivity of the density dependence to the shape of $V_2(r)$, which we have taken to be that of Eq. (18). This function accurately represents the static limit of meson theory for $r \gtrsim 1$ fm. So the only freedom in changing it is at small $r$, where meson theory is much less reliable. But for small $r$, the same arguments apply here as in the above discussion of short-range correlations. If $L \geq 1$ in $F_1$, or if $L+L' \geq 2$ in $F_2$, the region of small $r$ contributes little, and the precise shape of $V_2$ in this region is unimportant. If $L=0$ in $F_1$, or if $L=L'=0$ in $F_2$, the region of small $r$ may contribute appreciably to the integrals, but, for the reasons given earlier, this contribution will not change the density dependence. We conclude that the density dependence is insensitive to the behavior of $V_2(r)$ at small $r$.

We have seen at the end of Sec. V that, if we are to escape from the saturation band, then the energy shift must vary as $k_F^{8.5}$ or faster. According to Eqs. (84) and (90), this would require $L=3$ in the dispersion effect or $L=L'=3$ in the Pauli effect. However, for such large values of $L$ and $L'$, all energy shifts are too small to be of any interest. The reason is simply that, for large $L$, the functions $j_L(\bar{k}_0 r)$ that occur in Eqs. (82) and (88) are very small for all $r$ within the range of $V_2$.

The main conclusion of this subsection is that the energy shift due to $N\Delta$ coupling does not have a strong enough density dependence to move the system significantly out of the saturation band. This conclusion is independent of the presence or absence of a strong short-range repulsion in $V_1$, and it is insensitive to the shape of $V_2(r)$ at small $r$. Thus our main conclusion is model independent. The size of the energy shift due to $N\Delta$ coupling, however, is clearly model dependent.

### C. Coupling to other partial waves

We have given in Sec. V detailed numerical results for the couplings ${}^1S_0(NN) \rightleftarrows {}^5D_0(N\Delta)$ and ${}^3P_1(NN) \rightleftarrows {}^5P_1(N\Delta)$. In this subsection, we use the approximate formulas (71) and (73), divided by $(1+2\kappa)$, to estimate the loss of binding caused by other $N\Delta$ couplings. To apply the formulas, we must estimate $\kappa_{N\Delta}$ and $\kappa_P$ for each coupling. Since we have discussed the density dependence in the previous subsection, we work here only at the empirical Fermi momentum $k_F=1.36$ fm$^{-1}$. We also use the values $\bar{U}=-68$ MeV, $(\Delta-M)c^2=300$ MeV, and $\kappa=0.15$, which are appropriate for the RSC potential at $k_F=1.36$ fm$^{-1}$.

We consider first the remaining ${}^3P(NN) \rightleftarrows N\Delta$ couplings. For $N\Delta$ states with $L'=1$, we estimate $\kappa_{N\Delta}$ and $\kappa_P$ by using the results calculated for the coupling ${}^3P_1(NN) \rightleftarrows {}^5P_1(N\Delta)$, along with the assumption that $\kappa_{N\Delta}$ and $\kappa_P$ are both proportional to $\mathfrak{M}^2$ (see Table II for numerical values) and to the statistical weight $\nu=\frac{1}{8}(2J+1)(2T+1)$ of the $NN$ channel. For $N\Delta$ states with $L'=3$, we take $\kappa_P=0$, in accord with the discussion in the preceding subsection. To estimate $\kappa_{N\Delta}$ for $L'=3$, we have calculated it for the coupling ${}^3P_1(NN) \rightleftarrows {}^5F_1(N\Delta)$ by using Eq. (19) with $y=1$ for $V_2$, and the Reid ${}^3P_1$ potential for $V_1$ and $V_3$. This gives the value of $\kappa_{N\Delta}$ for $L'=3$, $\mathfrak{M}=2.683$, and $\nu=\frac{9}{8}$. The proportionality of $\kappa_{N\Delta}$ to $\mathfrak{M}^2\nu$ then determines its value for $L'=3$ and for other values of $\mathfrak{M}$ and $\nu$. It would have been better to adjust $V_1$ and $V_3$ to fit the ${}^3P_1$ phases, rather than simply using the Reid ${}^3P_1$ potential, but the value of $\kappa_{N\Delta}$ is not sensitive to such differences in the potential. We have tested this statement for the coupling ${}^3P_1(NN) \rightleftarrows {}^5P_1(N\Delta)$. The potential that fits the ${}^3P_1$ phases contains $V_2$ from Eq. (19) (with $y=1$) and $V_1$ and $V_3$ from column 2 of Table IV. The approximate calculation has the same $V_2$ but has the Reid ${}^3P_1$ potential for $V_1$ and $V_3$. The values obtained for $\kappa_{N\Delta}$ are 0.0052 and 0.0058, respectively, which differ by only 10%.

Thus we can estimate $\kappa_{N\Delta}$ and $\kappa_P$ for each of the ${}^3P(NN) \rightleftarrows N\Delta$ couplings listed in Table II. We then obtain the energy shifts from Eqs. (71) and (73), divided by $(1+2\kappa)$. The results are shown in Table VIII. Adding the shift of 1.7 MeV from Table VIII to the shift of 1.48 MeV for the coupling ${}^3P_1(NN) \rightleftarrows {}^5P_1(N\Delta)$ that can be read from Table V, we find, for $k_F=1.36$ fm$^{-1}$, a total shift of 3.2 MeV due to $P$-wave coupling. At the same value of $k_F$, the shift due to $S$-wave coupling is 3.3 MeV [the difference in Table V between the RSC+$\Delta(S)$ and the RSC+CORE($S$) energies]. Thus the combined effect of all $P$-wave couplings is comparable to that of the $S$-wave coupling.

TABLE VIII. Estimates of the loss in binding due to the ${}^3P(NN) \rightleftarrows N\Delta$ couplings [other than ${}^3P_1(NN) \rightleftarrows {}^5P_1(N\Delta)$] shown in Table II, at $k_F = 1.36$ fm$^{-1}$. The formulas used for these estimates are discussed in the text.

| $NN$ channel | $N\Delta$ channel | $\mathfrak{M}$ | $\nu(NN)$ | $\kappa_{N\Delta}$ | $\kappa_P$ | $\Delta\epsilon$ ($D$) (MeV) | $\Delta\epsilon$ ($P$) (MeV) | $\Delta\epsilon$ (tot) (MeV) |
|---|---|---|---|---|---|---|---|---|
| ${}^3P_0$ | ${}^3P_0$ | 1.333 | $\frac{3}{8}$ | 0.00043 | 0.00051 | 0.05 | 0.06 | 0.11 |
| ${}^3P_1$ | ${}^3P_1$ | −0.667 | $\frac{9}{8}$ | 0.00032 | 0.00038 | 0.04 | 0.04 | 0.08 |
| | ${}^5F_1$ | 2.191 | | 0.0060 | 0 | 0.31 | 0 | 0.31 |
| ${}^3P_2$ | ${}^3P_2$ | 0.133 | $\frac{15}{8}$ | 0.00002 | 0.00003 | 0.00 | 0.00 | 0.00 |
| | ${}^5P_2$ | −1.200 | | 0.0017 | 0.0021 | 0.20 | 0.24 | 0.44 |
| | ${}^3F_2$ | −0.980 | | 0.0020 | 0 | 0.10 | 0 | 0.10 |
| | ${}^5F_2$ | 2.400 | | 0.0120 | 0 | 0.63 | 0 | 0.63 |
| Total | | | | 0.0225 | 0.0029 | 1.33 | 0.34 | 1.67 |

From Tables VII and VIII, we find the total $P$-wave contribution to $\kappa_{N\Delta}$ to be about 0.028. Adding this to the $S$-wave contribution of 0.047 gives $\kappa_{N\Delta} \approx 0.075$. Thus at normal density each particle spends about 3.7% of its time as a Δ. This figure is expected to vary quadratically with the assumed strength of the $N\Delta$ coupling, i.e., it is expected to be proportional to $f^{*2}/4\pi$.

What about coupling of the ${}^1D_2(NN)$ state to $N\Delta$ states? Let us first consider $\kappa_{N\Delta}$ and note that with conventional nuclear forces, the ${}^1D_2$ contribution to $\kappa$ is more than 100 times smaller than the ${}^1S_0$ contribution.[27] Since the ${}^1D_2(NN) \rightleftarrows D(N\Delta)$ calculation involves [through Eq. (69)] matrix elements of the same type as in the conventional ${}^1D_2$ calculation, we expect that the coupling ${}^1D_2(NN) \rightleftarrows D(N\Delta)$ will contribute negligibly to $\kappa_{N\Delta}$. The coupling ${}^1D_2(NN) \rightleftarrows {}^5S_2(N\Delta)$ may be compared with the ordinary tensor coupling ${}^3D_1(NN) \rightleftarrows {}^3S_1(NN)$, which is also known[27] to contribute negligibly to $\kappa$. Thus we conclude that $\kappa_{N\Delta}$ is negligible, and we turn to consideration to $\kappa_P$. We have seen that only $N\Delta$ states with the smallest allowed value of $L'$ are important for $\kappa_P$, and we therefore consider only the coupling ${}^1D_2(NN) \rightleftarrows {}^5S_2(N\Delta)$. The relevant wound integral $I_P$ is given by Eq. (70), and the main contribution to the matrix element in the integrand is given by Eq. (77). In Eq. (77), when either $L = 2$ or $L' = 2$, the dominant contribution comes from large values of $r$, where $u_L(k_0, r) \approx r j_L(k_0 r)$. Hence, for a given potential $V_2(r)$, the matrix element (77) is roughly the same for the coupling ${}^1D_2(NN) \rightleftarrows {}^5S_2(N\Delta)$ as for the coupling ${}^1S_0(NN) \rightleftarrows {}^5D_0(N\Delta)$. Thus we expect $\kappa_P$ to be comparable for these two couplings, after due account is taken of the proportionality of $\kappa_P$ to $\mathfrak{M}^2$ and to $\nu = \frac{1}{8}(2J+1)(2T+1)$. From Table II, we find that $\mathfrak{M}^2\nu$ is the same for these two couplings. We then obtain the estimate, for the coupling ${}^1D_2(NN) \rightleftarrows {}^5S_2(N\Delta)$ at $k_F = 1.36$ fm$^{-1}$,

$$\Delta\epsilon(D) + \Delta\epsilon(P) \approx [-\bar{U} + \tfrac{1}{2}(\Delta - M)c^2]\,\kappa_P(1+2\kappa)^{-1} = 0.8 \text{ MeV} . \quad (91)$$

Here we used the value $\kappa_P = 0.0049$ that was calculated for the coupling ${}^1S_0(NN) \rightleftarrows {}^5D_0(N\Delta)$, along with the values $\bar{U} = -68$ MeV, $(\Delta - M)c^2 = 300$ MeV, and $\kappa = 0.15$. Thus we see that the effect of $D$-wave coupling to $N\Delta$ channels is small but not completely negligible. We expect the effects of all other couplings to be negligible.

## VII. SUMMARY

Our main result is that, although $N\Delta$ coupling causes a large reduction in binding energy, the density dependence of the energy shift does not move the system significantly off the saturation band. Our qualitative analysis shows that this conclusion is model independent. It does not depend on the short-range behavior of either $V_1$ or $V_2$, even though the size of the energy shift is model dependent.

It is difficult to escape the saturation band in the desired direction by means of *any* effect that reduces the binding energy. This is because, as was shown in Sec. V, a density dependence of $k_F^8$ or stronger is required. Therefore, the saturation properties of nuclear matter are more likely to be improved by an effect that increases the binding than by one that decreases the binding.

When $N\Delta$ coupling is added to the Reid potential at normal density, the reductions in binding energy from nucleon-nucleon $S$, $P$, and $D$ waves are 3.3, 3.2, and 0.8 MeV, respectively. For a given shape of the coupling potential $V_2$, we expect all of these figures to vary quadratically with the strength of $V_2$, i.e., linearly with $f^{*2}/4\pi$, where $f^*$ is the $\pi N\Delta$ coupling constant. We have used $f^{*2}/4\pi$

$=0.23$, as obtained from a quark model by Haapakoski.[25] But others[15-17] have used the value $f^{*2}/4\pi=0.35$ that is fitted to the observed width of the $\Delta$. We have seen that the $S$-wave energy shift is sensitive to the short-range behavior of the nucleon-nucleon potential $V_1$ and of the coupling potential $V_2$. If $V_2$ is large at short distances, then reducing the amount of short-range repulsion in $V_1$ will increase the loss of binding in the $^1S_0(NN)$ channel. The loss of binding in the $^3P(NN)$ and $^1D_2(NN)$ channels is much less sensitive to short-range correlations.

The probability $P_\Delta$ of a particle in nuclear matter being a $\Delta$ is $\frac{1}{2}\kappa_{N\Delta}$, where $\kappa_{N\Delta}$ is the contribution from the $N\Delta$ channel to the defect parameter $\kappa$. We have found $P_\Delta$ to be 3.7%, with 2.3% coming from the coupling $^1S_0(NN)\rightleftarrows{}^5D_0(N\Delta)$ and 1.4% from couplings of the type $^3P(NN)\rightleftarrows N\Delta$. For the coupling $^1S_0(NN)\rightleftarrows{}^5D_0(N\Delta)$, the energy shift is roughly proportional to $\kappa_{N\Delta}$, and $P_\Delta$ is therefore roughly proportional to the energy shift. So, for this coupling, $P_\Delta$ will show the same sensitivity to the short-range behavior of $V_1$ and $V_2$ as the energy shift. The contribution to $P_\Delta$ from the couplings $^3P(NN)\rightleftarrows N\Delta$ is much less sensitive to short-range correlations.

With the present model, including $N\Delta$ coupling in $S$, $P$, and $D$ waves at normal density reduces the binding energy by roughly 7 MeV. For the Reid potential this is very undesirable because the binding energy obtained from two-body correlations will then be only about 5 MeV, and it seems unlikely that three- and four-hole-line terms could raise this to the empirical value of 16 MeV. The $N\Delta$ coupling also causes an increase in the defect parameter $\kappa$. For $k_F=1.36$ fm$^{-1}$, the $S$-wave coupling increases $\kappa$ by 0.05 (see Table VII), and the combined effect of $P$-wave couplings is to increase $\kappa$ by 0.03 (see Tables VII and VIII). Since the ordinary Reid potential has $\kappa=0.14$, the $N\Delta$ coupling will increase this to 0.22 and appreciably worsen the convergence of the hole-line expansion.

Both of these undesirable effects could be ameliorated by adding $N\Delta$ coupling to a potential that saturates at too high a binding energy and density. The UG3 potential is just one example of this kind. Adding $N\Delta$ coupling to such a potential could produce in lowest-order Brueckner theory a value of $\kappa$ and a saturation point similar to those of the ordinary Reid potential without $N\Delta$ coupling. Then there would be a reasonable possibility that three- and four-hole-line corrections would move the saturation point into the empirical region.

## ACKNOWLEDGMENTS

We are grateful to F. J. D. Serduke for making his phase-shift-fitting program available to us. We thank P. Haapakoski for helpful correspondence and A. M. Green for communicating the results of Green and Niskanen before publication. We are also grateful to V. R. Pandharipande for sending his results for transition matrix elements, and to A. Bodmer, J. Rafelski, and S. Pieper for stimulating discussions.

*Work performed under the auspices of the U. S. Energy Research and Development Administration.

[1]B. D. Day, Rev. Mod. Phys. 39, 719 (1967).
[2]H. A. Bethe, Annu. Rev. Nucl. Sci. 21, 93 (1971).
[3]D. W. L. Sprung, *Advances in Nuclear Physics*, edited by M. Baranger and E. Vogt (Plenum, New York, 1972), Vol. 5.
[4]C. W. Wong and T. Sawada, Ann. Phys. (N.Y.) 72, 107 (1972).
[5]F. Coester, S. Cohen, B. Day, and C. M. Vincent, Phys. Rev. C 1, 769 (1970).
[6]M. I. Haftel and F. Tabakin, Phys. Rev. C 3, 921 (1971).
[7]P. K. Banerjee and D. W. L. Sprung, Can. J. Phys. 49, 1899 (1971).
[8]H. S. Köhler, Nucl. Phys. A204, 65 (1973).
[9]J.-P. Jeukenne, A. Lejeune, and C. Mahaux, Nucl. Phys. A245, 411 (1975).
[10]V. R. Pandharipande, R. B. Wiringa, and B. D. Day, Phys. Lett. 57B, 205 (1975).
[11]T. K. Dahlblom, in *Proceedings of the Abo Academy* (NORDITA, Blegdamsvej 17, Copenhagen, Denmark), Ser. B, Vol. 29, No. 6.
[12]P. Grange, Phys. Lett. 56B, 439 (1975).
[13]B. D. Day, Phys. Rev. 187, 1269 (1969).
[14]F. Coester, S. C. Pieper, and F. J. D. Serduke, Phys. Rev. C 11, 1 (1975).
[15]A. M. Green and T. H. Schucan, Nucl. Phys. A188, 289 (1972).
[16]A. M. Green and P. Haapakoski, Nucl. Phys. A221, 429 (1974).
[17]A. M. Green and J. A. Niskanen, Nucl. Phys. A249, 493 (1975).
[18]A. R. Bodmer and D. M. Rote, Nucl. Phys. A169, 1 (1971).
[19]Y. Nogami and E. Satoh, Nucl. Phys. B19, 91 (1970).
[20]R. V. Reid, Ann. Phys. (N.Y.) 50, 411 (1968).
[21]T. Ueda and A. E. S. Green, Phys. Rev. 174, 1304 (1968).
[22]H. Sugawara and F. Von Hippel, Phys. Rev. 172, 1764 (1968).
[23]A. R. Edmonds, *Angular Momentum in Quantum Mechanics* (Princeton U. P., Princeton, 1960).
[24]R. A. Smith and V. R. Pandharipande, Nucl. Phys. A256, 327 (1976).
[25]P. Haapakoski, Phys. Lett. 48B, 307 (1974).
[26]S. C. Pieper, Phys. Rev. C 9, 883 (1974).
[27]A. Kallio and B. D. Day, Nucl. Phys. A124, 177 (1969).
[28]T. Hamada and I. D. Johnston, Nucl. Phys. 34, 382 (1962).
[29]V. R. Pandharipande, Nucl. Phys. A181, 33 (1972).
[30]H. A. Bethe, B. H. Brandow, and A. G. Petschek, Phys. Rev. 129, 225 (1963).
[31]P. Haapakoski and M. Saarela, Phys. Lett. 53B, 333 (1974).